Electronic structure of ordered and disordered Cu_3Au and Cu_3Pd

Z. W. Lu, S.-H. Wei, and Alex Zunger
National Renewable Energy Laboratory, Golden, Colorado 80401
(Received 2 January 1992)

In ordered $L1_2$-type A_3B compounds, each A atom is coordinated by $8A + 4B$ atoms, while each B atom is coordinated by $12A$ atoms. By symmetry, all A-A, A-B, and B-B bond lengths are equal. When this structure disorders to form the substitutionally random $A_{0.75}B_{0.25}$ alloy, each atom acquires a *distribution* of different types of coordination shells. Concomitantly with this reduction in site symmetries, (i) topologically different A atoms (and separately, different B atoms) can have unequal charges, and (ii) the various bonds need not be of equal average lengths $\langle R\rangle$ (i.e., $\langle R_{A\text{-}A}\rangle \neq \langle R_{A\text{-}B}\rangle \neq \langle R_{B\text{-}B}\rangle$). Furthermore, (iii) there can be a distribution of bond length values around $\langle R_{ij}\rangle$ for each of the three chemical bond types. In this work we study the effects of such charge fluctuations (i) and relaxational fluctuations [(ii) and (iii)] on the electronic structure of Cu_3Au and Cu_3Pd. The random alloys are modeled by the special quasirandom structure (SQS), whereby the sites of a periodic supercell are occupied by A and B atoms so that the first few radial correlation functions closely reproduce the average correlation functions in an infinite substitutional random network. Instead of requiring that each atom "see" an identical, average medium, as is the case in the homogeneous site-coherent-potential approximation (SCPA), we thus create a distribution of distinct local environments whose average corresponds to the random alloy. Application of a first-principles local-density method (linearized augmented-plane-wave method) to the SQS then provides the energy-minimizing equilibrium relaxations, charge density, density of states, and formation enthalpy. We find that charge and relaxational fluctuations neglected in the SCPA lead to a significant stabilization of the alloy ($\sim$ 30% lowering in mixing enthalpy) and to substantial ($\sim$ 1 eV) nonrigid shifts in the electronic energy levels.

I. INTRODUCTION

The class of Cu_3X intermetallic compounds with X = Pd, Pt, and Au undergo as a function of temperature a phase transition between the low-temperature ordered $L1_2$ phase (Fig. 1) and the high-temperature disordered $Cu_{0.75}X_{0.25}$ phase.[1-4] This type of phase transition is particularly interesting, since the chemical identity of the coordination sphere about the Cu and X sites changes significantly through the transition. This can be seen as follows: The ordered $L1_2$ structure consists of four interpenetrating simple cubic lattices i, of which $i = 1$, 2, and 3 are occupied by Cu, whereas $i = 4$ is distinct and is occupied by X. In this structure all Cu atoms, and separately all X atoms are crystallographically equivalent, and there is a single, unique $R_{Cu-Cu} = R_{Cu-X} = R_{X-X}$ bond of length $R = a/\sqrt{2}$, where a is the cubic lattice constant. On the other hand, in the high-temperature disordered phase, all four sublattices can be occupied by Cu and X. The probability $P(\alpha/i)$ that atom of type α (=Cu or X) occupies sublattice i is

$$P(\mathrm{Cu}/i) = \frac{3}{4}, \quad P(X/i) = \frac{1}{4}. \tag{1}$$

Consistent with these site probabilities the disordered phase exhibits a *distribution* of generally *inequivalent* atom pairs (as well as triangles, tetrahedra, etc.). Figure 1(c) illustrates this for the random disorder limit, showing a significant change in the number of like neighbors around an atom through the transition: In the disordered phase, each atom (Cu or X) is coordinated on average by $3X$ + 9Cu, while in the ordered $L1_2$ phase Cu is coordinated by $4X$ + 8Cu and X is coordinated by 12 Cu atoms. These values are average coordinations; Fig. 1(c) shows that the distribution is wide, so many other arrangements are also probable in the random alloy. For instance, 4.0%, 10.3%, and 19.4% of the Cu atoms are coordinated by 6, 7, and 8 Cu atoms, respectively. Such changes in the chemical identity of the coordination shell of the ordered vs disordered phases can drive concomitant fluctuations in the charge distributions and atomic relaxations. This should be contrasted with the $L1_1 \leftrightarrow$ disordered transformation at $x = \frac{1}{2}$ (seen, e.g., in $Cu_{0.5}Pt_{0.5}$), where the average coordination of Cu and X (6Cu+6X) is unchanged through the transition, as shown in Fig. 1(d). We have previously presented a first-principles thermodynamic theory for the energetics of these types of phase transitions.[5,6] Here we investigate the changes in *electronic structure* attendant upon the Cu_3X ($L1_2$) $\leftrightarrow$ $Cu_{0.75}X_{0.25}$ order-disorder transition for X = Pd and Au, using the same first-principles approach. We will focus on the changes induced by the creation of a distribution of local environments in the disordered phase.

Mean-field theories[7,8] (e.g., the single-site coherent approximation, or SCPA) describe such $A_{1-x}B_x$ alloys by

 ©1992 The American Physical Society

replacing the distribution of many inequivalent local environments [Fig. 1(c)] by a *uniform medium* of identical "effective" sites with which atoms A and B interact. There are but two distinct average potential functions (one for A, one for B). At each given composition all A atoms (and separately, all B atoms) are taken to be equivalent. Hence, in averaging over all local environments, the homogeneous SCPA removes all *geometrical* aspects of the problem, retaining the average *topology* of the underlying Bravais lattice. This leads to the assumption of (i) equal average bond lengths $R_{A-A} = R_{A-B} = R_{B-B}$ in the disordered system and (ii) equal charge on all A atoms (and separately, B atoms), irrespective of the chemical identity of the sites surrounding the atom locally (e.g., A surrounded by A's are assumed to have the same charge as A surrounded by B's).

We have used instead a real-space description of the *geometry* of the alloy: sites are occupied by A's and B's so that the radial correlation functions of a small supercell reproduce, by design, the first few (configurationally averaged) correlation functions of an infinite, random $A_{1-x}B_x$ network at a given x. If one desires to mimic deviations from perfect randomness (i.e., short-range order), the correlation functions of the special quasirandom structure (SQS) can be fit to finite-temperature results obtained from a thermodynamic model. In either cases, the electronic properties of such special quasirandom structures[9,10] can then be solved by ordinary self-consistent band-theoretical approaches. Hence, instead of requiring that each atom "see" an identical, average medium, we create a *distribution* of distinct environments whose average corresponds to the random medium. The limitation of the methods lies in the fact that with a small-size supercell one can correctly reproduce the geometrical atomic arrangements only within a few bond lengths from each site. While this was shown[9–11] to be better than what can be achieved with ordinary (rather than "special") supercells whose sites are occupied *at random* ("coin flip") by A's and B's, physical properties that depend sensitively on long-range correlations (e.g., intensities of x-ray diffraction[10]) cannot be accurately reproduced by small SQS's. Our experience[9,10] suggests, however, that many interesting alloy properties (equilibrium bond lengths, local density of states, charge transfer, formation enthalpies, etc.) depend primarily on the existence of many distinct *local* environments in the disordered phase, rather than on the details of the long-range correlation functions. The second limitation of the method is that small-size SQS's exist only for "principal compositions" such as $x = \frac{1}{4}$, $\frac{1}{2}$, and $\frac{3}{4}$; arbitrary compositions can be modeled only by impractically large SQS's. However, consideration of such principal compositions (along with the results at $x = 0$ and 1) often captures most of the relevant aspects of the electronic structure.

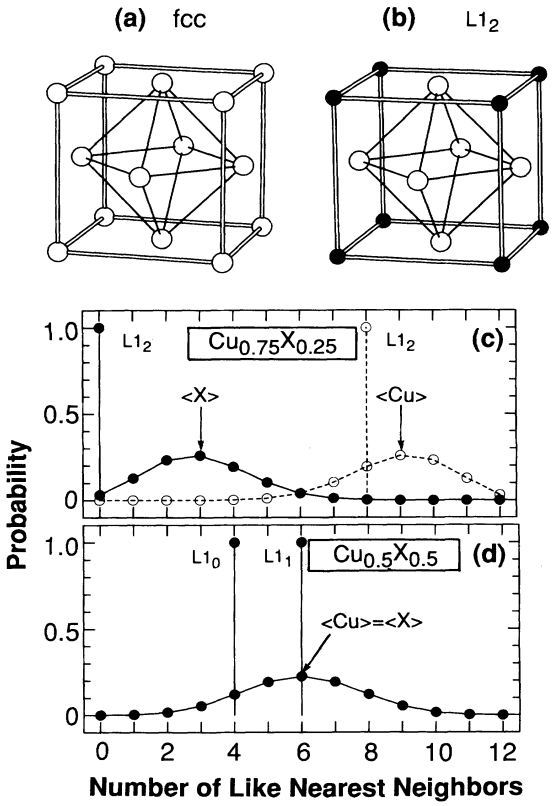

FIG. 1. (a) Crystal structures of the face-centered-cubic (fcc) and (b) $L1_2$ structures. (c) and (d) show the probabilities of finding a given number of like neighbors to Cu (open circles) and X (solid circles) in the random (c) $Cu_{0.75}X_{0.25}$ alloys and (d) $Cu_{0.5}X_{0.5}$ alloys. The vertical lines in (c) and (d) show the result for ordered structures. Values in angular brackets give the average coordination in the random alloys.

We will apply the SQS to a self-consistent local-density description as implemented by the general potential linearized augmented-plane-wave (LAPW) method.[12] This produces equilibrium atomic positions, total energy, density of states, and charge density. We find that the existence in the random alloy of a distribution of crystallographically inequivalent sites [Fig. 1(c)] leads to a concomitant distribution of electronic charges and bond lengths. This leads to significant ($\sim$ 1 eV) nonrigid shifts in the density of states, substantial lowering in the mixing enthalpies (by $\sim$ 30%) that are missed by the homogeneous SCPA. A preliminary brief account of this work appeared recently.[13]

II. ELECTRONIC HAMILTONIAN AND ITS SOLUTION

A. Details of computations for ordered compounds

We calculate the electronic properties of the alloy in the local-density approximation[14,15] (LDA) using Wigner's exchange correlation potential.[16] The LDA equations were solved by the LAPW method,[12] in which fully self-consistent solutions to the effective single-particle equations are found, without restricting the shape of the potential and charge density. Inside the muffin-tin (MT) spheres, the nonspherical charge density and potential were expanded in terms of lattice harmonics of angular momentum $l \leq 8$. The muffin-tin radii used here are $R_{\mathrm{MT}}^{\mathrm{Cu}} = 1.164$ Å, $R_{\mathrm{MT}}^{\mathrm{Pd}} = 1.270$ Å, and

R_{MT}^{Au} = 1.302 Å. A basis set of 70–90 LAPW's/atom are used (equivalent to kinetic-energy cutoffs of 13.2 Ry for Cu-Au and 16.7 Ry for Cu-Pd). During the self-consistency iterations, the Brillouin-zone summation was done using 60 special **k** points[17] in the irreducible zone for the fcc constituents and 20 special **k** points for the ordered $L1_2$ structure. The calculations were carried out scalar relativistically for Cu-Pd and Cu-Au, as well as fully relativistically for the Cu-Au system. The densities of states (DOS's) were calculated using the tetrahedron integration method.[18] The resulting DOS's were then smoothed using a Gaussian function with a full width at half maximum of about 0.2 eV. The energy eigenvalues were evaluated at 195 and 120 **k** points in the irreducible Brillouin zone for the fcc and the $L1_2$ structures, respectively.

B. Results for the fcc constituents

Figure 2 depicts the DOS of fcc elemental Cu, Pd, and Au at their calculated equilibrium lattice parameters (solid lines) and at the lattice parameters appropriate to that of Cu_3X (dashed lines). The scalar-relativistic (SR) and nonrelativistic (NR) equilibrium lattice parameters of the pure fcc solids are given in Table I. The calculated SR lattice parameters are seen to be within 0.4% of the experimental values[19] for Pd and Au, while for Cu (having the most localized d states) the error is 1.5%. Our underestimation of the lattice parameter of Cu will also render the lattice parameters of Cu_3X smaller than experiment.[4,20] In all cases, relativistic correction reduces the lattice parameter. Interestingly, relativistic mass velocity and Darwin effects can also significantly modify the calculated bulk moduli of heavy-atom solids: For fcc Au (in Mbar)

$$B_{SR}(Au) = 1.83, \quad B_{NR}(Au) = 1.19 \ , \tag{2}$$

while for fcc Pt (in Mbar)

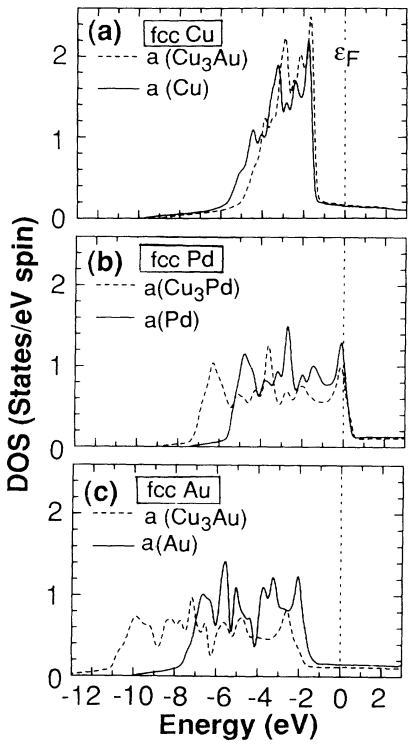

FIG. 2. Density of states of the fcc elemental solids: (a) Cu at the a_{SR} = 3.562 Å (solid line) and at a = 3.709 Å corresponding to the equilibrium value of Cu_3Au (dashed line). (b) Pd at the a_{SR} = 3.882 Å (solid line) and at a = 3.648 Å corresponding to the equilibrium value of Cu_3Pd (dashed line). (c) Au at the a_{SR} = 4.094 Å (solid line) and at a = 3.709 Å corresponding to the equilibrium value of Cu_3Au (dashed line).

$$B_{SR}(Pt) = 2.87, \quad B_{NR}(Pt) = 1.80 \ . \tag{3}$$

Relativistic effects, hence, stiffen the bulk moduli by ~ 40%, largely due to the reduction in atomic sizes of the heavy atoms.

TABLE I. Calculated equilibrium lattice constants (a_{eq}) and formation enthalpies (ΔH) in the nonrelativistic (NR) and scalar-relativistic (SR) approaches for the $L1_2$ structures and the fcc constituents. $\bar{a}$ is the Vegard's rule value of Eq. (4). ΔH_{SR} for Cu_3Pd and Cu_3Au were calculated at the eqilibrium SR lattice constant, whereas ΔH_{NR} were calculated at the NR $\bar{a}$ values.

	a_{eq} (Å)			ΔH (meV/atom)	
System	NR	SR	Expt.	NR	SR
Cu	3.608	3.562	3.615[a]		
Pd	3.937	3.822	3.890[a]		
Au	4.286	4.094	4.078[a]		
$\bar{a}(Cu_3Au)$	3.801	3.709			
$\bar{a}(Cu_3Pd)$	3.696	3.648			
Cu_3Au		3.720	3.743[b]	+149.9	−42.5
Cu_3Pd		3.650	3.674[c]	−90.3	−85.0

[a] Reference 19: room-temperature data.
[b] Reference 4: room-temperature data.
[c] Reference 20: room-temperature data.

III. ELECTRONIC STRUCTURE AND PROPERTIES OF THE $L1_2$ ORDERED COMPOUNDS

A. Formation enthalpies and lattice parameters

Table I shows the equilibrium lattice constants and formation enthalpies for ordered Cu_3Au and Cu_3Pd in the $L1_2$ structure. The calculated SR equilibrium lattice constants for Cu_3Au and Cu_3Pd are within 0.5% and 0.1% of Vegard's rule

$$\bar{a} = \left(\frac{(3V_{Cu} + V_{Au})}{4}\right)^{\frac{1}{3}}. \quad (4)$$

Our ~1% underestimation of the lattice parameters of the $L1_2$ compound is largely due to the corresponding LDA error in describing the lattice parameter of fcc Cu (Table I).

Our calculated formation enthalpy for Cu_3Pd is close to the result of Takizawa and Terakura [−78 meV/atom, using the augmented-spherical-wave[21] (ASW) method and the von Barth–Hedin exchange-correlation potential[22]]. Our calculated formation enthalpy for Cu_3Au is 7.4 meV lower than our result in Refs. 5 and 6, where a larger basis cutoff was used. It is also close to the result of Davenport, Watson, and Weinert[23] of −48 meV/atom [obtained by using the linear augmented-Slater-type-orbital (LASTO) method, and the Hedin-Lunqvist exchange correlation potential[24]]. The negative values of ΔH of Cu_3Pd and Cu_3Au indicate that these systems are stable in the $L1_2$ structures with respect to phase separation. Our previous survey of the ground states of these systems[5,6] have further shown that the $L1_2$ structure is in fact a ground-state structure for both Cu-Pd and Cu-Au, in agreement with experiment.[1–4]

The increase in the lattice mismatch between the Cu and Au in the nonrelativistic calculation relative to the scalar-relativistic case suggests an increase in the elastic strain energy of the $L1_2$ system. Indeed, the calculated nonrelativistic formation enthalpy of Cu_3Au ($L1_2$) is *positive*, showing that relativity stabilizes the ordered phase with respect to phase separation. We find similar a trend for Ni-Pt.[25] On the other hand, the nonrelativistic formation enthalpy of Cu_3Pd is rather similar to the calculated scalar-relativistic value.

B. Trends with X in the electronic structure of the Cu_3X $L1_2$ structures

The electronic structure of $L1_2$ *ordered* Cu_3Pd (Refs. 26–28) and Cu_3Au (Refs. 23, 27, and 29–51) is reasonably well understood owing to the many theoretical[23,26,27,29–37] and experimental[34–51] studies of these systems. In order to articulate the issues we want to address in the context of the order ↔ disorder transition, we first describe the basic electronic structure of the *ordered* phase. We will illustrate the main points using both our LAPW results for Cu_3Au and Cu_3Pd as well as literature results for other systems. Figures 3 and 4 show the DOS's and the atom-projected DOS's of the $L1_2$ forms of Cu_3Au and Cu_3Pd, respectively.

One finds in general that the "solute" atom X can create deep bonding states near the bottom of the Cu d band as well as antibonding states near the top of the host d band. The relative positions depend largely on the relative d-orbital binding energies as follows.

(i) When the d-orbital energy of X is considerably deeper than that of Cu [e.g., X=Au or Zn (Ref. 52)], the X-like bonding state appears as a separate band below the Cu d band [a "split band" bonding state, denoted as "B" in Fig. 3(a)], whereas the X-like antibonding (AB) state appears as a hybridized state, resonating within the

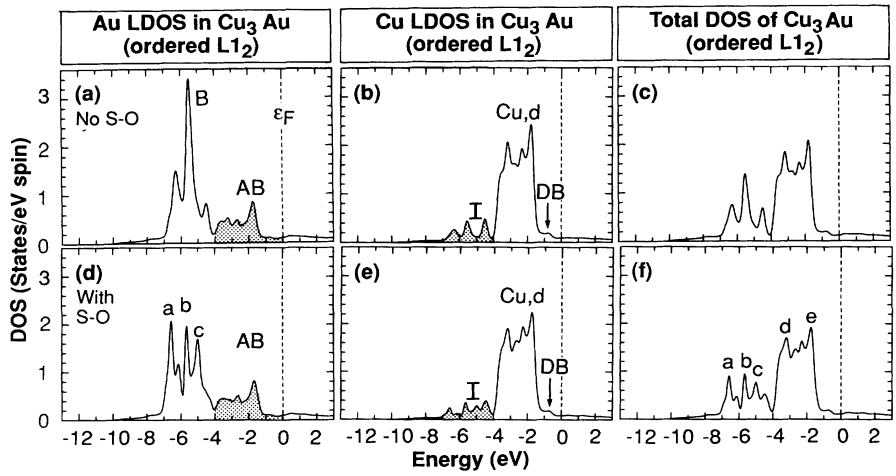

FIG. 3. DOS of ordered $L1_2$ Cu_3Au (a) inside the Au muffin-tin spheres (b) inside the Cu muffin-tin spheres. (c) Total DOS in the whole space. The calculation was carried out at $\bar{a}$ = 3.709 Å. Results for (a)–(c) are scalar relativistic (without spin-orbit effects). Panels (d)–(f) show the corresponding results including spin-orbit effects. The capital letters denote type of states: B=bonding, AB=anti-bonding, I=induced, DB=dangling bond (see text). The lower-case letters *a*, *b*, *c*, *d*, and *e* denote peak positions whose energies are given in Table III.

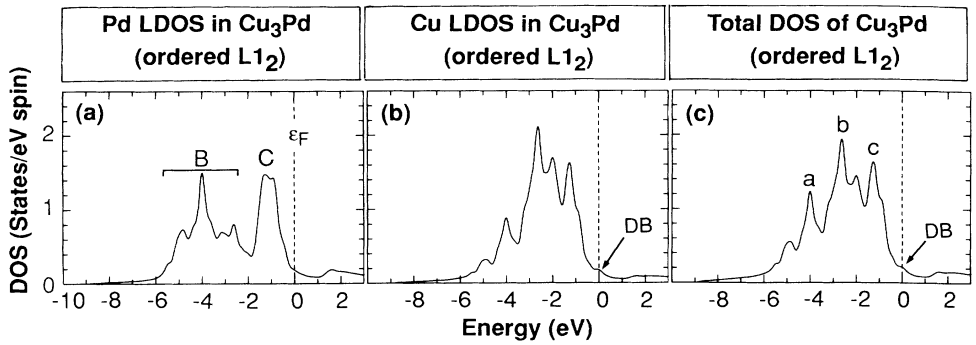

FIG. 4. DOS of ordered $L1_2$ Cu_3Pd (a) inside the Pd muffin-tin spheres (b) inside the Cu muffin-tin spheres. (c) Total DOS in the whole space. The scalar-relativistic calculation was carried out at $\overline{a} = 3.648$ Å. The capital letters denote type of states: B=bonding, AB=anti-bonding, I=induced, DB=dangling bond, C=common band (see text). The lower-case letters *a*, *b*, *c*, *d*, and *e* denote peak positions whose energies are given in Table II.

Cu *d* band, near its top ["common band" antibonding state, denoted "AB" in Fig. 3(a)]. This state can also be thought of as the consequence of Cu orbitals penetrating the region of the X atom. Similarly, the penetration of the wave function tails of X into the region of Cu induces an X-like state in Cu local density of states [denoted "I" in Fig. 3(b)]. The Cu *d* band remains largely unperturbed except for a vacancylike dangling-bond state [denoted "DB" in Fig. 3(b)]. Figure 5 shows the charge densities in $L1_2$ Cu_3Au, confirming the dominant bonding character of band B [Fig. 5(a), where the density lobes point *toward* the nearest neighbors], the antibonding character of the AB band [Fig. 5(b), where the density lobes point *between* the nearest neighbors], and the dangling-bond-like characters of DB [Fig. 5(c), where the wave function is highly localized on Cu, with vanishing amplitude on the Au sites].

(ii) Considering next the opposite limit, where the *d* orbital of X are nearly equally bound as those of Cu *d* [e.g., X=Ni (Ref. 53)], one finds that the bonding state B has moved up into the Cu band, while the previously resonating states DB are expelled by the Cu-X *d-d* repulsion and appear above the Cu *d* band.

(iii) In the intermediate case [e.g., X=Pd (Ref. 13)], one finds the bonding state near (or inside) the Cu *d* band [denoted "B" in Fig. 4(a)], a common, mixed Cu-Pd band [denoted "C" in Fig. 4(a)] and the dangling-bond state above the Cu *d* band [denoted "DB" in Fig. 4(b)]. The charge-density contours (not shown) substantiate this assignment.

The calculations discussed so far are scalar-relativistic, i.e., they include mass-velocity and Darwin effects, but omit spin-orbit corrections. The latter are important for heavy atoms, e.g., for X=Au. The results of a fully relativistic calculation are shown in Figs. 3(d)–3(f). One finds (i) a splitting of the Au-like bonding states "B" [Fig. 3(d)] into $J = \frac{5}{2}$ and $\frac{3}{2}$ states, with a smaller effect on the *d* band of the lighter atom Cu states [Fig. 3(e)], (ii) The Au-induced states in the Cu LDOS [denoted "I" in Fig. 3(e)] carry the Au spin-orbit fingerprints, while the Cu-induced states in the Au LDOS [denoted "AB" in Fig. 3(d)] carry the Cu spin-orbit signature, i.e., are nearly unchanged by spin-orbit effects.

There are many previous investigations of the electronic structure of the Cu_3Au system. Tables II and III list positions (relative to the Fermi energy) of the prominent densities of states peaks of the ordered $L1_2$ Cu_3Pd and Cu_3Au, respectively. Our result is in generally good agreement with previous theoretical studies. Comparison with x-ray photoemission spectroscopy (XPS) and ultraviolet photoemission spectroscopy (UPS) shows that the LDA underestimates the binding energies of peaks *a*–*e* in Fig. 3(f) (with respect to the Fermi energy) by 0.4–0.8 eV, as also noted in previous investigations.[31,37,47]

C. Evolution of the electronic structure of A_3B from A and B

Contrasting the electronic structure of Cu_3X with that of the constituents ("Cu_3Cu" and "X_3X") one finds the following effects.

1. *Volume deformation effects*

Since the partial molar volumes in Cu_3X are intermediate between that of "Cu_3Cu" and "X_3X," the element with the smaller molar volume expands in the alloy environment while that with the larger elemental volume contracts. These uniform, hydrostaticlike effects change band positions and widths. Since both Pd and Au are larger than Cu (the observed relative lattice constant mismatches are 7% and 11%, respectively), we expect that compression of Au and Pd in Cu_3Au and Cu_3Pd, respectively, will displace their bonding states to *deeper* binding energies and *broaden* their *d* bands. This expectation is confirmed by Fig. 2, where the DOS of fcc Pd and Au are shown both at their calculated equilibrium fcc lattice constants and at the lattice constant appropriate to Cu_3X (assuming Vegard's rule). The Pd *d* band widens from 5.6 to 7.4 eV and the Au *d* band widens from 5.6 to 8.8 eV. Conversely, dilation of Cu in the alloy environment will displace its *d* band to *shallower* binding energies and *narrow* its *d* bands. This volume effect on the more localized Cu 3*d* orbitals is much smaller than that on the more diffused 4*d* Pd and 5*d* Au. This is seen in Fig. 2(a): The Cu *d* band narrows by 0.6 eV as the

lattice parameter changes from the equilibrium Cu value to the lattice constant appropriate for Cu_3Au.

2. Site occupation effects

While in the pure fcc solids atoms are coordinated only by like species [Fig. 1(a)], in the $L1_2$ Cu_3X structure the X atom is coordinated solely by Cu atoms. Consequently, the larger atom X-X overlap is reduced in the $L1_2$ structure so its subbands are expect to narrow, much like "quasi-impurity states." For Cu this effect on the subbands is much smaller. Note that the volume deformation and site-occupation effects are opposite for the X sublattice (broadening and narrowing, respectively).

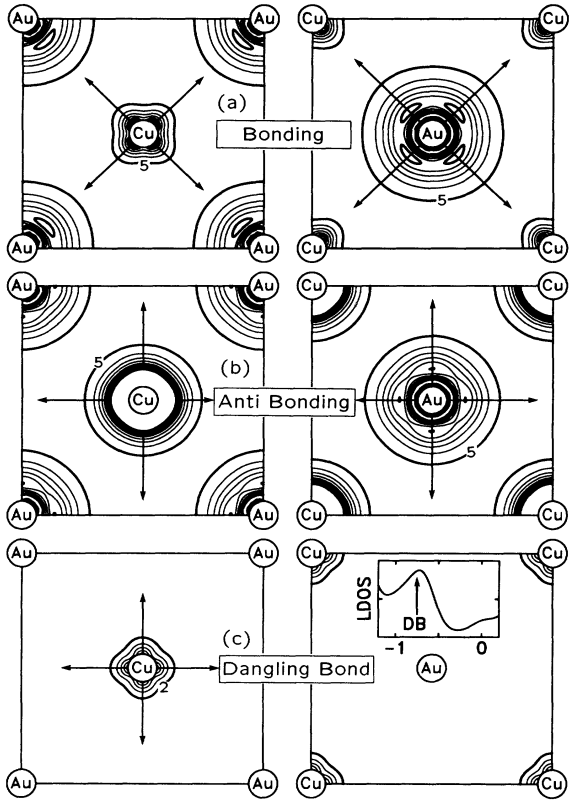

FIG. 5. Charge density contour plots for $L1_2$ Cu_3Au calculated fully relativistically. (a) Charge density corresponding to the energy range between −4.0 and −7.0 eV below ε_F. This includes the Au bonding state [denoted "B" in Fig. 3(d)] and the Au-induced Cu states [denoted "I" in Fig. 3(e)]. (b) Charge density corresponding to energy range between −1.0 eV to −4.0 eV below ε_F. This includes the Au antibonding states [denoted "AB" in Fig. 3(d)] and the Cu d band states [denoted Cu, 3d in Fig. 3(e)]. (c) The Cu impurity-like dangling-bond state [denoted "DB" in Fig. 3(e)] corresponding to the energy range between −0.5 and −1.0 eV. The insert to Fig. 5(c) shows on an enlarged scale the dangling bond LDOS peak of Fig. 3(e). Lattice constant $\bar{a} = 3.709$ Å. Contours are labeled in units of 10^{-2} e/a.u.^{3} The contour increment is 5×10^{-2} e/a.u.^{3}, except in (c) where it is 2×10^{-2} e/a.u.^{3} The arrows in this figure show the direction in which the prominent components of the charge density point.

TABLE II. Comparison of the density of states peak positions (with respect to the Fermi energy, in eV) of the ordered Cu_3Pd with other calculations. The peaks a, b, and c are shown in Fig. 4(c).

Peak	a	b	c
Present[a]	4.0	2.6	1.3
LMTO[b]	4.0	2.8	1.5
APW[c]	3.5	2.7	1.3

[a]Calculated at the lattice constant $a = 3.648$ Å.
[b]Reference 26 using the fully relativistic LMTO method.
[c]Reference 28 using the APW method.

3. Charge-transfer effects

The difference $\Delta\rho(\mathbf{r})$ of the charge density in a compound and that of its solid elemental constituents

$$\Delta\rho^{(\alpha)} = \rho_{\text{compound}}(\mathbf{r}) - \rho^{(\alpha)}_{\text{fcc}}(\mathbf{r}) \tag{5}$$

can affect the electronic states. It is generally accepted that in a given system $\Delta\rho^{\alpha}(\mathbf{r})$ is largest for sites α coordinated by *unlike* atoms, while when α is coordinated mostly by like atoms $\Delta\rho^{\alpha}(\mathbf{r})$ is smaller. We, hence, expect a significant charge rearrangement at the X site in Cu_3X (since X is coordinated only by Cu atoms), and a smaller rearrangement at the Cu site (coordinated by $4X$ atoms).

Transfer of electronic charge onto (off) an atom raises (lowers) the Coulomb repulsion on that site, hence reducing (increasing) the binding energy of states whose wave functions are localized mostly with that site. This effect can be partially offset by the interatomic Madelung effect: Transfer of charge off sublattice A onto sublattice B creates a repulsive Coulomb effect on B but also diminishes the Coulomb potential on that site due to the field created there by the oppositely charged sublattice A. Because of this partial cancellation, we will see below that despite a marked difference in charge transfer on different A (or B) atoms, the effect on the electronic states can be small.

D. Expected changes in electronic structure in the $L1_2 \leftrightarrow$ disorder transition

There are a number of previous calculations of the electronic structure of disordered $Cu_{0.75}Pd_{0.25}$ (Refs. 26–28 and 54–57) and $Cu_{0.75}Au_{0.25}$ (Refs. 27, 31, 33, 34, and 58–60). All are based on the "site-coherent-potential approximation" (SCPA). They vary in detail: The underlying electronic Hamiltonian can be of the tight-binding form[28,54,55,57] or the density functional form (Refs. 26, 27, 31, 33, 34, 56, and 58–60); the charge density is either made self-consistent[26,31,56,59] or frozen at the form in the ordered structure,[27,34,60] and the Hamiltonian is treated nonrelativistically,[58] scalar relativistically,[26,33,34,59] or

fully relativistically.[27,31,58,60] In all cases the average bond distances are taken to be equal $R(\text{Cu}-X) = R(\text{Cu}-\text{Cu}) = R(X-X)$ and all atoms of a given chemical type are assumed to have the same potential and charge distribution (so the Madelung energy is taken to be zero).

Our foregoing discussion clarifies the aspects of the electronic structure that are likely to change when the $L1_2$ structure disorders.

(i) In so far as the lattice constant of the disordered $Cu_{0.75}X_{0.25}$ alloy is close to that of the ordered Cu_3X compounds, no additional "volume deformation effects" are to be expected. Experimental data on lattice-constant changes through the phase transition show that the difference in lattice constant between the ordered and disordered is less than 0.3%.[4]

(ii) The changed average site occupancies in the disordered phase relative to the ordered structure [Fig. 1(c)] can lead to a small reduction in charge transfer for Cu (coordinated in the alloy by nine Cu atoms, as opposed to eight Cu atoms in the ordered compound) and more so for X (coordinated in the alloy, on average, by three X atoms, as opposed to none in the ordered compound). Only the *average* occupation effect is included in a SCPA description of the alloy.

(iii) The existence in the disordered phase of a *distribution* of inequivalent Cu sites (and separately, inequivalent X sites) can lead to a concomitant distribution of charges on chemically identical atoms. This could lead to additional structure in the alloy's DOS relative to that of the $L1_2$ structure. The SCPA method does not describe this distribution. As discussed in Sec. III C 3, the partial cancellation between the intrasite and intersite Coulomb effects can minimize the effect of such charge fluctuations on the DOS.

(iv) The crystallographic inequivalence of chemically identical atomic sites in the disordered alloy can lead to a distribution of bond lengths. Recent extended x-ray-absorption fine structure (EXAFS) exper-

TABLE III. Comparison of the energy of peaks a–e [Fig. 3(f)] (with respect to the Fermi energy, in eV) in the density of states of the ordered Cu_3Au with experiment and other calculations. Peaks a, b, c, d, and e are shown in Fig. 3(c).

	a	b	c	d	e
			Calculations		
Present[a]	6.5	5.6	4.9	3.1	1.7
Present[b]	6.3	5.4	4.8	3.0	1.7
LMTO[c]	6.9	5.7	4.9		2.2
LAPW[d]	6.1	5.4	4.2	3.1	1.7
LASTO[e]	6.2	5.4	4.3	3.1	1.8
LMTO[f]	6.5	5.6	4.8	3.1	1.7
			Experiment		
XPS[g]	6.8	5.8			2.4
UPS[h]	6.9	6.0	5.1	3.3	2.5
UPS[i]	6.3		5.3		2.5
XPS[j]	6.9	5.6			2.5
UPS[k]	6.4		5.1		2.6
UPS[l]	6.8–7.0	6.0–6.1	4.8–5.0		2.3
UPS[m]	6.9	6.3		3.7	2.6

[a]Calculated at the lattice constant $a = 3.709$ Å: the calculated Vegard's lattice constant.

[b]Calculated at the experimental lattice constant of 3.7426 Å (Ref. 4).

[c]Reference 37 calculated using a linear muffin-tin orbital (LMTO) method.

[d]Reference 36 calculated scalar relativistically using a LAPW method at $a = 3.748$ Å using the Wigner XC potential.

[e]Reference 23 calculated scalar relativistically using a LASTO method at $a = 3.741$ Å using the Hedin-Lunqvist XC potential.

[f]Reference 31 calculated fully relativistically using a LMTO method at $a = 3.7478$ Å using the von Barth–Hedin XC potential.

[g]Reference 49 using an x-ray-photoelectron diffraction (XPS) technique at the photon energy $\hbar\omega = 1253.6$ eV.

[h]Reference 47 using ultraviolet-photoelectron spectroscopy (UPS) at the photon energy $h\nu = 26$ eV.

[i]Reference 46 using the UPS technique at photon energy $h\nu = 40$ eV.

[j]Reference 45 using the XPS technique at the photon energy $h\nu = 1486.6$ eV .

[k]Reference 44 using the UPS technique at the photon energy $h\nu$ between 30 and 160 eV.

[l]Reference 37 using the UPS technique at the photon energy $h\nu$ between 22 and 80 eV.

[m]Reference 36 using the UPS technique at photon energy $h\nu = 75$ eV.

iments on $Ni_{1-x}Au_x$ (Ref. 61) and on dilute Pd in Cu (Ref. 62) demonstrated this point. It has been previously shown that analogous "bond-relaxation" effects in $(AC)_{1-x}(BC)_x$ semiconductor alloys can lead to substantial changes in the electronic structure relative to hypothetical "unrelaxed" lattice[10] assumed in SCPA calculations. Our foregoing discussion of the basic electronic structure $L1_2$ compounds points to the way that such nonhydrostatic atomic distortions will couple to the electronic states: Bonding states [e.g., "B" in Figs. 3(a) and 4(a)] will be displaced into deeper (shallower) binding energies when the corresponding bond distances are shortened (elongated) by relaxation, while the reverse is to be expected for antibonding states. The homogeneous SCPA description of alloys does not consider relaxation effects.

IV. SQS DESCRIPTION OF THE RANDOM PHASE

A. Structural information

We have previously applied the SQS method to study the electronic structures at $x = \frac{1}{2}$ for some intermetallic systems[63] and semiconductor alloys.[9,10] Here, we will apply the SQS concept to study the electronic structure of $x = \frac{1}{4}$ and to some extent, $x = \frac{1}{2}$ intermetallic alloys. We have previously specified the structure of the SQS at $x = \frac{1}{2}$: It can be described as an $A_1B_2A_3B_2$ superlattice along the [113] direction. The $x = \frac{1}{4}$ (or $x = \frac{3}{4}$) alloy is described by the SQS consisting of A_6B_2 layers stacked along the $[\bar{1}02]$ direction. It has the monoclinic unit cell [space group C_{2h}^1 (Ref. 64)] with lattice vectors

$$\begin{aligned} \mathbf{a} &= (\ 0.0,\ 1.0,\ 0.0)a, \\ \mathbf{b} &= (\ 1.0,\ 0.5,\ 0.5)a, \\ \mathbf{c} &= (-1.0, -0.5,\ 1.5)a\ , \end{aligned} \tag{6}$$

where a is the cubic lattice constant. The ideal (unrelaxed) atomic positions for SQS-$\frac{1}{4}$ in Cartesian coordinates are

$$\begin{aligned} A^{(7)} &= (\ 0.5,\ 0.0,\ 0.5)a,\ \ (-1.0,\ 0.0,\ -1.0)a, \\ A^{(9)} &= (-1.0,\ 0.0,\ 0.0)a,\ \ (\ 0.5,\ 0.0,\ -0.5)a, \\ A^{(11)} &= (-0.5,\ 0.0,\ 0.5)a,\ \ (\ 0.0,\ 0.0,\ -1.0)a, \\ B^{(3)} &= (\ 0.0,\ 0.0,\ 0.0)a,\ \ (-0.5,\ 0.0,\ -0.5)a\ . \end{aligned} \tag{7}$$

Here, the numbers in superscript denote the number of like atoms in the nearest-neighbor shell. We list the lattice-average spin products (defined in Ref. 5) $\overline{\Pi}_{k,m}$ for k-body mth neighbor correlation functions for SQS-$\frac{1}{4}$ in Table IV, showing that the SQS-$\frac{1}{4}$ mimics reasonably well the correlation functions of the infinite random alloy at the same composition. Note that "periodicity errors" (due to the use of periodic boundary conditions in the SQS) are included in $\overline{\Pi}_{k,m}$ so $\overline{\Pi}_{k,m}(\mathrm{SQS}) - \overline{\Pi}_{k,m}(\mathrm{random})$ of Table IV already reflects these errors.

In applying the LAPW to SQS we have used 96 special **k** points for Cu-Pd and 24 **k** points for Cu-Au for the Brillouin-zone integration. The DOS was calculated using 93 **k** points in the irreducible Brillouin zone.

B. Structural relaxation of the SQS and alloy mixing enthalpies

Disordered $A_{1-x}B_x$ alloys are characterized by a variety of local atomic environments and can have distinct A–A, A–B, and B–B bonds. Furthermore, even within the same type of bond, there is a distribution of bond lengths as seen by the EXAFS experiments.[61] The relaxed geometry of the alloy is determined here from first-principles total-energy minimization on the respective SQS's at the alloy's volume $V(x)$ maintaining the overall cubic-cell structure. While straightforward, the large number of cell-internal structural degrees of freedom make this calculation computer intensive; hence, there is a premium on finding a reasonable initial guess. This can be done by realizing that the SQS's can also be described as "superlattices" along some special orientations $\mathbf{G} \| [lmn]$, and that continuum elasticity theory[65] provides the equilibrium spacing along $\mathbf{G}$ as a function of the externally fixed lattice constant $a_\perp$ perpendicular to $\mathbf{G}$ as

$$c_{\mathrm{eq}}^{(\lambda)}(a_\perp) = a_{\mathrm{eq}}^{(\lambda)} - [2 - 3q_\lambda(\mathbf{G})][a_\perp - a_{\mathrm{eq}}^{(\lambda)}]\ , \tag{8}$$

where $a_{\mathrm{eq}}^{(\lambda)}$ is the cubic lattice constant of material λ. Here, $q_\lambda(\mathbf{G})$ is the "strain reduction factor" along $\mathbf{G}$ given by[65] $q(\mathbf{G}) = 1 - B/[C_{11} + \gamma(\mathbf{G})\Delta]$, where $\Delta = C_{44} - (C_{11} - C_{12})/2$ is the elastic anisotropy, B is the bulk modulus, C_{ij} are the elastic constants and the orientation dependence is given by the geometric constant

$$\gamma(\mathbf{G}) = \frac{4(l^2m^2 + m^2n^2 + n^2l^2)}{(l^2 + m^2 + n^2)^2}\ , \tag{9}$$

e.g., $\gamma(001) = 0$, $\gamma(201) = \frac{16}{25}$, and $\gamma(113) = \frac{76}{121}$. While the elemental solids Cu and X have the equilibrium lattice constants $a_{\mathrm{eq}}^{(\lambda)}$, in the alloy environment these will expand and contract, respectively, to the alloy value $a_\perp = a(x)$. We then imagine a coherent layer of pure Cu (or X) whose lattice constant is constrained to equal the alloy value $a(x)$ in the direction perpendicular to $\mathbf{G}$,

TABLE IV. The lattice average spin products $\overline{\Pi}_{k,m}$ for k-body mth neighbor correlation functions for SQS-$\frac{1}{4}$ and for the random alloy at same composition $[(\overline{\Pi}_{k,m})_{\mathrm{R}} = (2x-1)^k]$.

Structure	$\overline{\Pi}_{0,1}$	$\overline{\Pi}_{1,1}$	$\overline{\Pi}_{2,1}$	$\overline{\Pi}_{3,1}$	$\overline{\Pi}_{4,1}$	$\overline{\Pi}_{2,2}$	$\overline{\Pi}_{2,3}$	$\overline{\Pi}_{2,4}$
SQS-$\frac{1}{4}$	1	$-\frac{1}{2}$	$\frac{1}{4}$	$-\frac{1}{4}$	$\frac{1}{2}$	$\frac{1}{3}$	$\frac{1}{4}$	0
Random	1	$-\frac{1}{2}$	$\frac{1}{4}$	$-\frac{1}{8}$	$\frac{1}{16}$	$\frac{1}{4}$	$\frac{1}{4}$	$\frac{1}{4}$

finding from Eqs. (8) and (9) the Cu–Cu (or X–X) interlayer distances parallel to G. We then layer these Cu and X planes in the SQS, finding the corresponding Cu and X atomic position so that the interlayer distances match those obtained above. We have applied this elastic model to the SQS, obtaining an initial guess for the relaxed atomic positions. This is then refined by minimizing the LAPW total energy with respect to all atomic positions keeping the overall unit cell cubic. This is done by calculating the quantum-mechanical forces using the method of Yu, Singh, and Krakauer.[66] We find that the fully relaxed geometry is rather close to that predicted by the simple elastic model: The average bond lengths changed by less than 0.5% and the total energy was reduced by less than 2 meV/atom.

We find that the mixing enthalpy $\Delta H_{\rm mix}(x)$ of the disordered alloy $Cu_{1-x}Pd_x$ was reduced significantly by relaxation; denoting unrelaxed by UR and relaxed by R, we find for $x = \frac{1}{2}$ (in meV/atom),[67]

$$\Delta H^{\rm UR}_{\rm mix}(\tfrac{1}{2}) = -45.0, \quad \Delta H^{\rm R}_{\rm mix}(\tfrac{1}{2}) = -62.5 \ , \tag{10}$$

while for $x = \frac{1}{4}$ (in meV/atom),

$$\Delta H^{\rm UR}_{\rm mix}(\tfrac{1}{4}) = -28.6, \quad \Delta H^{\rm R}_{\rm mix}(\tfrac{1}{4}) = -50.3 \ . \tag{11}$$

The SR "ordering energy"

$$\Delta E_o(x) = \Delta H(L1_2) - \Delta H_{\rm mix}(x = \tfrac{1}{4}) \tag{12}$$

at $x = \frac{1}{4}$ changes upon relaxation from -56.4 to -34.7 meV/atom. Clearly, atomic relaxations (absent by symmetry in the ordered $L1_2$ Cu_3X compound and neglected in previous SCPA alloy calculations) are very significant in a size-mismatch disordered alloy. We next examine the consequences of these energy lowerings on the atomic structure of the alloy.

V. DISTRIBUTION OF BOND LENGTHS IN DISORDERED ALLOY

Figure 6 displays the calculated relaxed bond lengths in $Cu_{1-x}Pd_x$ and $Cu_{1-x}Au_x$ (each averaged, for convenience of display over its distribution). Three features are noteworthy: (i) All bond lengths deviate both from the "ideal" values in the pure constituents; they also deviate from the common "virtual-lattice" values

$$R = \frac{\sqrt{2}}{2}[(1-x)a_{\rm Cu} + xa_X] \tag{13}$$

(shown as the dotted diagonal line in Fig. 6), assumed in all SCPA calculations. (ii) The *width* ($\sim$ 0.05 Å) of the distribution for each bond type in $Cu_{1-x}Pd_x$ is comparable to the difference in the average bond lengths, e.g., the difference $\langle R_{\rm Pd-Pd}\rangle - \langle R_{\rm Cu-Cu}\rangle$ is 0.078, 0.073, and 0.069 Å at $x = \frac{1}{4}$, $\frac{1}{2}$, and $\frac{3}{4}$, respectively. This can also be seen in Table V where we list the average bond lengths and the standard deviations for $Cu_{0.5}Pd_{0.5}$ and $Cu_{0.5}Au_{0.5}$. (iii) The bond lengths in the random alloy are significantly different from those in the ordered $L1_0$ or $L1_2$ compounds at the same composition x_c [e.g., at $x = \frac{1}{4}$ the bond lengths for the $L1_2$ structure are $(\sqrt{2}/2)a(x)$].

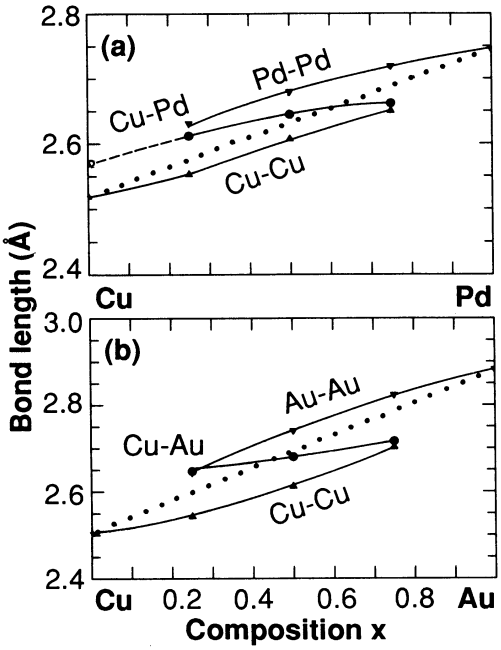

FIG. 6. Average bond lengths in $Cu_{1-x}Pd_x$ and $Cu_{1-x}Au_x$. The diagonal dotted line gives the virtual lattice average of Eq. (13). Calculated points (joined by lines to guide the eye) represent average over distributions whose standard deviations are 0.052 and 0.050 Å for Pd-Pd at $x = \frac{1}{4}$ and $x = \frac{1}{2}$ and 0.052 and 0.063 Å for Cu-Pd at the same compositions. The open circle denotes the extrapolated Cu-Pd bond length for dilute $Cu_{0.99}Pd_{0.01}$ alloy. It is found to be 2% larger than the Cu-Cu distance in pure Cu.

We fitted the calculated Cu–Pd bond lengths at $x = \frac{1}{4}$, $\frac{1}{2}$, and $\frac{3}{4}$, to a parabolic function. By extrapolating the result to the dilute limit $x = 0$ [open circle in Fig. 6(a)], we found that there is a Cu–Pd bond-length expansion of 2% around a Pd impurity, in good agreement with EXAFS experiment[62] giving a 2.0% expansion.

TABLE V. The calculated average bond lengths $\bar{d}$ and their standard deviations δd for $Cu_{0.5}Pd_{0.5}$ and $Cu_{0.5}Pd_{0.5}$ in units of Å.

$\bar{d}$	δd	$\bar{d}$	δd	$\bar{d}$	δd
Cu–Cu		Cu–Pd		Pd–Pd	
2.606	0.050	2.645	0.063	2.680	0.045
Cu–Cu		Cu–Au		Au–Au	
2.660	0.078	2.720	0.109	2.788	0.086

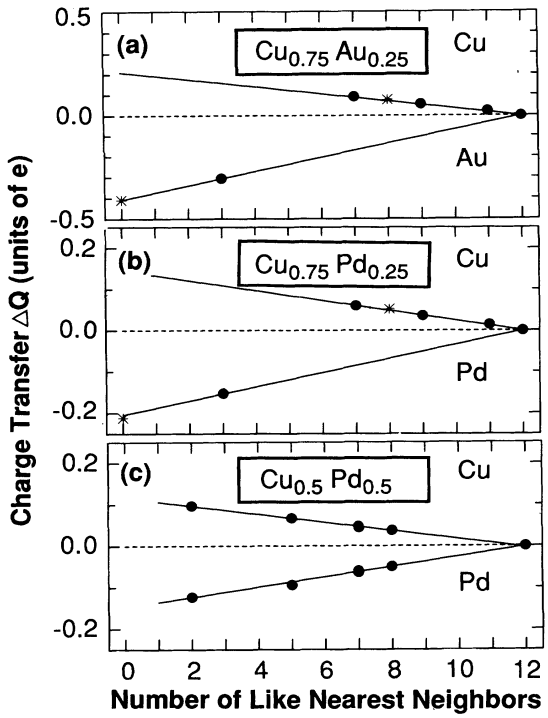

FIG. 7. Integrated total-charge transfer inside the muffin-tin spheres of unrelaxed (a) $Cu_{0.75}Au_{0.25}$ and (b) $Cu_{0.75}Pd_{0.25}$. (c) $Cu_{0.5}Pd_{0.5}$ with respect to the pure fcc solids as a function of the number of like atoms in the first coordination shell. The asterisks denote values for the atoms in the ordered $L1_2$ structure; solid symbols are for atoms in the SQS.

VI. CHARGE TRANSFER

Self-consistent local-density calculations of the electronic structure of (ordered or disordered) compounds provide in a natural way the energy-minimizing electronic charge density $\rho(\mathbf{r})$. While this quantity is unique, attempts to characterize it in terms of charge transfer between the subunits of the compound (e.g., atomic spheres) are clearly arbitrary in that there is no unique or compelling way to apportion a three-dimensional solid into simple subunits. Correlating such a charge transfer with the (thermochemically derived) Pauling electronegativity scale[68] is, hence, problematic precisely because of the arbitrariness in defining the subunits that exchange charge.[69] Nevertheless, experiments and calculation give information about the actual distribution of charge in the solid and the "apparent" charge transfer. Here, we will discuss the charge transfer in an alloy according to the definition of Eq. (5).

Figure 7 depicts the total charge transfer of Eq. (5) integrated within the muffin-tin spheres as a function of the number of like nearest neighbors for Cu-Pd and Cu-Au. Solid symbols are for the various atoms in the SQS, whereas asterisks give the values from the ordered $L1_2$ compounds. One notices the following.

(i) Relative to the elemental solids, Cu gains charge, whereas the more electronegative[68] Pd and Au *lose charge*. Hence, global charge transfer occurs from the fcc partner with the higher total density to the one with the lower total electron density, irrespective of the thermochemical electronegativity values.[68] This observation also applies to the Ag-Au and Ag-Pd systems studied previously.[63] This trend was also observed experimentally by Sham *et al.*[51] for the Cu-Au alloys and by Hedman *et al.*[70] for the Cu-Pd alloys.

(ii) As noted in Sec. III C 3, chemically identical but crystallographically inequivalent sites experience different magnitudes of charge transfer. Figure 7 confirms this expectation, showing that the amount of charge transfer indeed depends linearly[63,71] on the number of *unlike* nearest neighbors. Hence, the Au atom coordinated in the $L1_2$ structure by 12 Cu atoms with no Au neighbor

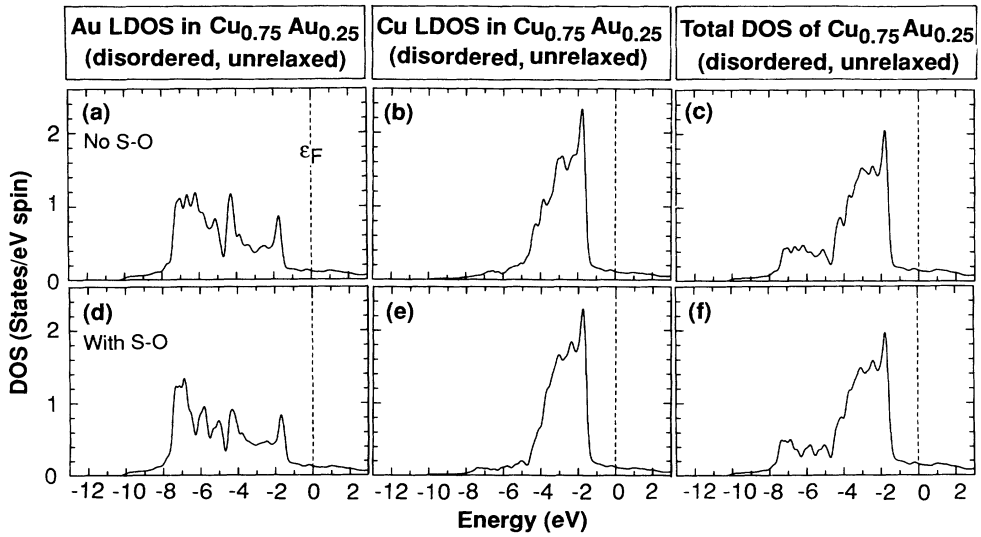

FIG. 8. Density of states of the *unrelaxed* disordered $Cu_{0.75}Au_{0.25}$: (a) and (d) inside the Au muffin-tin spheres, (b) and (e) inside the Cu muffin-tin spheres, and (c) and (f) total DOS in the whole space. The results in (a)–(c) were calculated semirelativistically (spin-orbit effect is not included), while results in (d)–(f) were performed fully relativistically (spin-orbit effect included). The calculation was done at lattice constant $\bar{a} = 3.709$ Å.

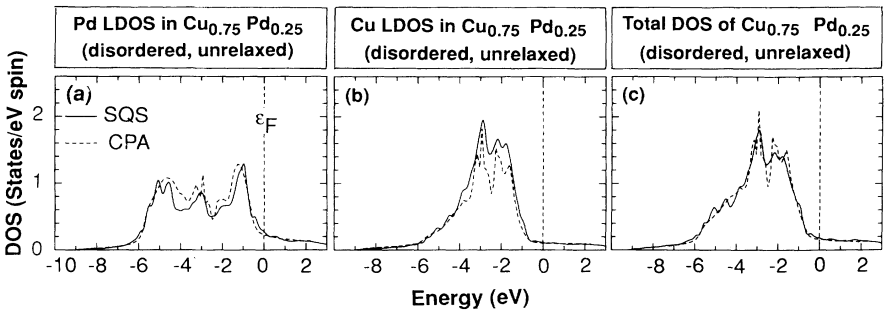

FIG. 9. Scalar-relativistic density of states of the unrelaxed disordered $Cu_{0.75}Pd_{0.25}$. (a) The Pd LDOS inside the muffin-tin spheres, (b) Cu LDOS inside the muffin-tin spheres, and (c) total DOS in the whole space. The solid line is the present LAPW result applied to SQS-$\frac{1}{4}$, while the dashed line gives the KKR-CPA result of Ginatempo *et al.*[27]

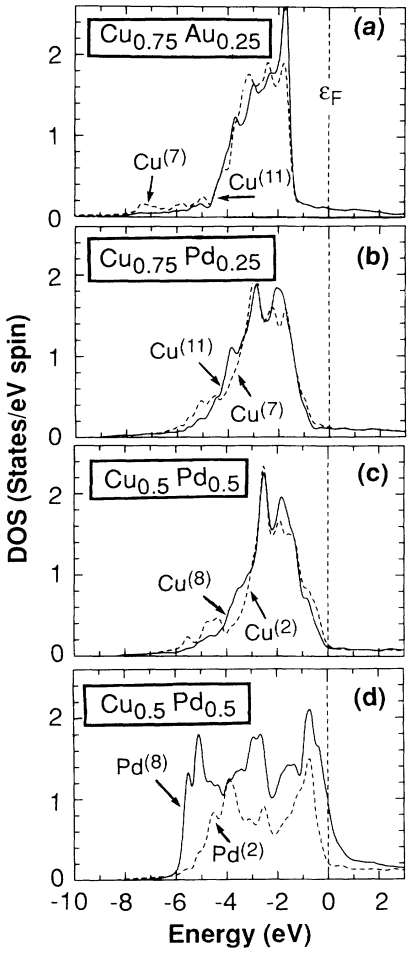

FIG. 10. "Environmental effects" on the DOS showing atom-centered DOS's. This gives the local density of states inside the MT spheres for (a) $Cu^{(7)}$ and $Cu^{(11)}$ in the $Cu_{0.75}Au_{0.25}$ SQS, (b) $Cu^{(7)}$ and $Cu^{(11)}$ in the $Cu_{0.75}Pd_{0.25}$ SQS, (c) $Cu^{(2)}$ and $Cu^{(8)}$ in the $Cu_{0.5}Pd_{0.5}$ SQS, and (d) $Pd^{(2)}$ and $Pd^{(8)}$ in the $Cu_{0.5}Pd_{0.5}$ SQS. The superscripts denote the number of like atoms in the nearest-neighbor shell. Note in (d) that Pd coordinated locally by only two Pd atoms has a narrower DOS than Pd coordinated by eight Pd atoms. These effects are weaker for the more compact Cu atoms.

loses the most charge, while the Au atom in the alloy coordinated by three Au atoms loses less charge. Note that the results of the SQS and those for the ordered $L1_2$ compounds fall on the same line, suggesting that the magnitude of charge transfer at a given global composition reflects largely *short*-range correlations. The same linearity of charge vs number of like neighbors was previously found for $Ag_{0.5}Au_{0.5}$, $Ag_{0.5}Pd_{0.5}$, and $Cu_{0.5}Pd_{0.5}$ alloys in Ref. 63. The values of the slope (λ) of such lines should be only half of those quoted there in the text. The SCPA assumes, on the other hand a constant charge on all atoms at a given global composition. This yields spuriously a zero Madelung energy. Our linear model of Fig. 7 has been used previously to study the electrostatic Madelung energy of the fcc lattices,[71] showing a finite electrostatic energy.

Recent Au $L_{2,3}$-edge x-ray-absorption near-edge structure measurement by Sham *et al.*[51] indicated that Au loses "5*d* count" upon compound formation both in ordered and disordered phases, but that there is a greater loss of *d* charge in forming the ordered $L1_2$ phase than in forming the disordered phase. This could be understood in light of Fig. 7(a): The Au atom is coordinated

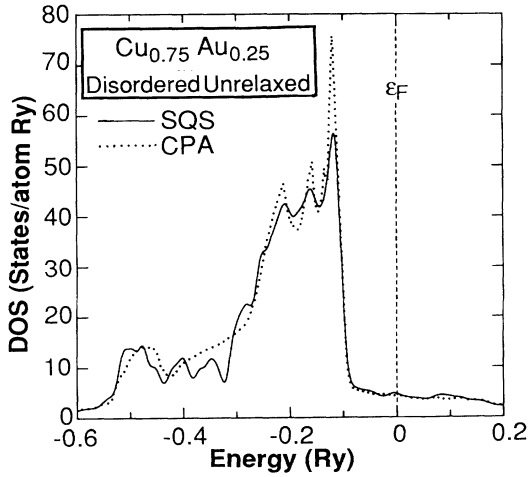

FIG. 11. Comparison of the present unrelaxed DOS obtained from the SQS (solid line) and the unrelaxed KKR-CPA calculation by Ginatempo and Staunton (Ref. 60) (dashed line) for $Cu_{0.75}Au_{0.25}$.

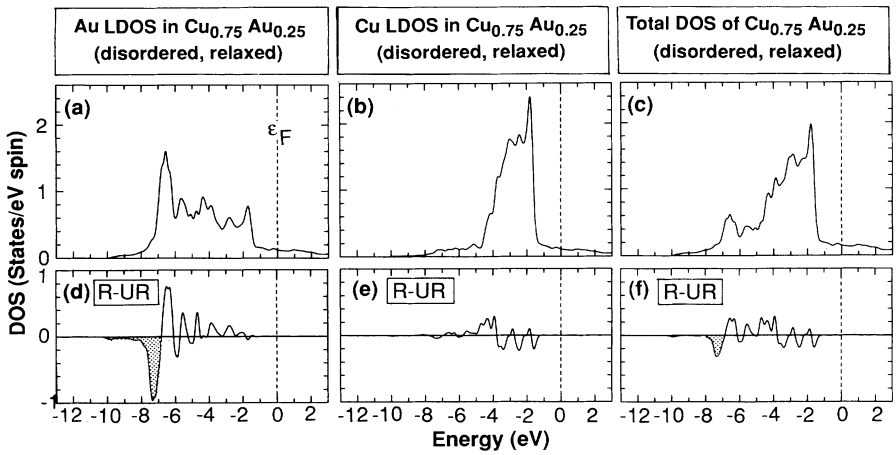

FIG. 12. (a)–(c) give the density of states of the relaxed disordered $Cu_{0.75}Au_{0.25}$. (a) LDOS inside the Au muffin-tin spheres. (b) LDOS inside the Cu muffin-tin spheres. (c) total DOS in the whole space. (d)–(f) shows the corresponding LDOS difference between the relaxed (R) and unrelaxed (UR) geometries. The fully relativistic calculation was carried out at $\bar{a} = 3.709$ Å.

in the $L1_2$ structure only by Cu atoms; hence, it loses the most charge. On the other hand, in the disordered phase, the Au atom is coordinated on average by three Au and nine Cu atoms; hence, it loses less charge than in the ordered $L1_2$ phase. Sham *et al.* further suggest a Au $5d$ charge-transfer value of -0.25 and -0.23 electrons for ordered and disordered phases, respectively. This order of magnitude is confirmed by our first-principles calculation where we find that the Au $5d$ (not the total charge transfer) charge loss is -0.21 and -0.17 electrons within the muffin-tin sphere for the ordered and the disordered phases, respectively. The Au $5d$ charge loss is smaller in the unrelaxed calculation for the disordered phase (-0.15 electrons). These values naturally depend on the muffin-tin radius; hence, they provide only semiquantitative trends.

VII. DENSITY OF STATES FOR DISORDERED ALLOYS

A. General description

The Cu-Au system shows the so-called "split-band" behavior. This can be illustrated using the ordered $L1_2$ Cu_3Au as an example. The Au local density of states (LDOS) [Fig. 3(d)] is isolated mostly at the high binding energy between -4.0 to -8.0 eV below ε_F and the Au band width narrows with respect to the elemental fcc Au (Fig. 2). The Cu LDOS is isolated in the energy range between -1.0 to -4.0 eV below ε_F. This split-band behavior is also evident in the disordered $Cu_{0.75}Au_{0.25}$ alloy as illustrated in Fig. 8, where the Cu DOS features are seen to maintain the general shape and width as in the ordered $L1_2$ phase [Fig. 3(e)]. This is consistent with the fact that the compact Cu $3d$ orbitals are rather insensitive to the changed local environment in the order-disorder transition and that, in addition, the Cu coordination is not changed much as $L1_2$ disorders: The Cu atoms have eight Cu nearest neighbors in the $L1_2$ structure and an average of nine Cu nearest neighbors in the disordered phase [Fig. 1(c)]. In contrast, the Au LDOS changes significantly through the transition: The sharp peaks a, b, c in the $L1_2$ structure [Fig. 3(d)] are smeared in the alloy [Fig. 8(d)] and the bonding-antibonding gap is reduced. This reflects the fact that the more delocalized Au $5d$ orbitals are better able to sense the changed local environment through the transition, and that the local environment as seen from the point of view of the Au atom changes significantly through the transition [Fig. 1(c)], from zero to three Au neighbors.

Figures 8(d)–8(f) display the effects of spin-orbit coupling on the DOS of the unrelaxed disorded $Cu_{0.75}Au_{0.25}$ alloy. The spin-orbit coupling affects the LDOS of the heavy Au atom most drastically in the Au bonding region [-4.0 to -8.0 eV below ε_F in Figs. 8(a) and 8(d)] but negligibly for the lighter $3d$ Cu atom [Figs. 8(b) and 8(e)].

While Cu-Au shows split-band behavior, Cu-Pd is a common-band system in the energy range ε_F to $\varepsilon_F - 6$ eV as seen in the results of the ordered phase (Fig. 4), where the Cu and Pd atoms features are intermixed. This common band behavior can also be inferred from the DOS of the elemental constituents (Fig. 2), where the DOS's of Cu and Pd are seen to overlap. When the $L1_2$ system disorders (Fig. 9) the DOS changes substantially [e.g., peak a in the $L1_2$ shown in Fig. 4(c) is attenuated in the disordered alloy, seen in Fig. 9(c)], while retaining this common band behavior. Again, the changes are more evident in the spectral range characteristic of the extended Pd states than in the range reflecting the more localized Cu states.

B. Effect of local environments in the unrelaxed alloy

Figure 1(c) shows that in the disordered alloy there is a distribution of local geometrical environments about chemically identical species. Figure 7 shows that different local environments lead to different charges on chemically identical species, and Fig. 6 shows that these fluctuations

drive symmetry-lowering lattice distortions. To examine the consequences of local environments on the LDOS, we show in Fig. 10 the Cu LDOS in $Cu_{0.75}Au_{0.25}$ alloy from the point view of different Cu atoms in the SQS. For example, Fig. 10(a) shows the results for Cu coordinated by eleven Cu nearest neighbors ($Cu^{(11)}$) and for Cu coordinated by only seven Cu nearest neighbors ($Cu^{(7)}$). We see that Cu LDOS is rather insensitive to the local environment [Figs. 10(a)–10(c)], reflecting the high degree of localization of the Cu orbitals (e.g., see Fig. 5). On the other hand, the more extended Pd orbitals clearly sense their local environments, as seen in Fig. 10(d): The $Pd^{(2)}$ site surrounded mostly by Cu atoms has a larger charge transfer [Fig. 7(c)] and narrower bandwidth [Fig. 10(d)] than the $Pd^{(8)}$ site.

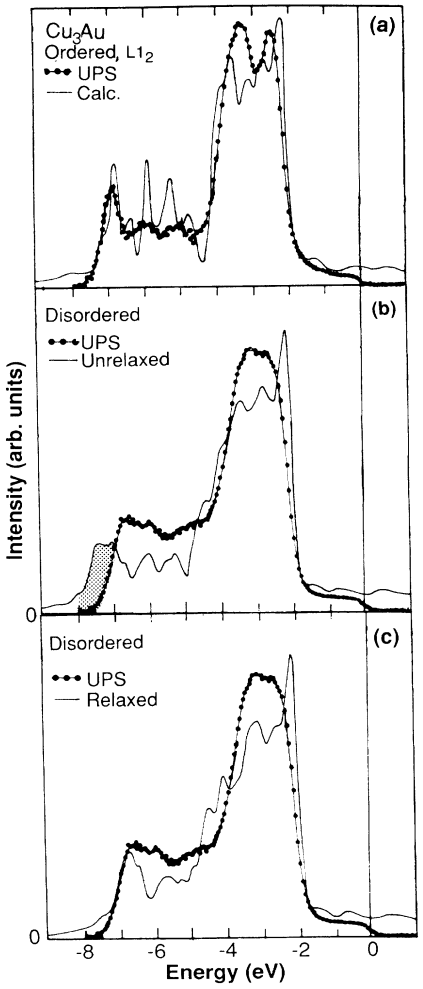

FIG. 13. Comparison between our fully relativistic DOS and the measured valence band photoemission (UPS) (Ref. 47) for Cu_3Au. The thin lines represent the calculated results, while the connected dotted lines represent the experimental results. (a) The ordered $L1_2$ Cu_3Au calculated at $a = 3.743$ Å. (b) The unrelaxed $Cu_{0.75}Au_{0.25}$ DOS calculated at $a = 3.755$ Å. (c) The relaxed $Cu_{0.75}Au_{0.25}$ DOS calculated at $a = 3.755$ Å. The shaded area in (b) highlights the $\sim$ 1-eV discrepancy with experiment, which is rectified by including relaxation (c).

C. Comparison of unrelaxed DOS with previous calculations

1. $Cu_{0.75}Au_{0.25}$

We next compare our calculated unrelaxed DOS with previous, equally unrelaxed Korringa-Kohn-Rostoker coherent-potential-approximation (KKR-CPA) calculations.[27,60] All of our previous discussion centered on the results at the calculated lattice constant $\bar{a} = 3.709$ Å, which is about 1% smaller than the experimental lattice constant $a = 3.755$ Å.[4] Since previous DOS calculations have used the experimental lattice constant, we have recalculated fully relativistically the DOS of $Cu_{0.75}Au_{0.25}$ alloy at the experimental lattice constant. Figure 11 compares our *unrelaxed* total DOS with the earlier (equally unrelaxed) KKR-CPA calculation of Ginatempo and Staunton.[60] The results are strikingly similar in the Cu region, but we observe additional structure in the present SQS calculation at the top of the Au band, near $\varepsilon_F - 0.4$ Ry. The close similarity in the Cu region reflects the insensitivity of the Cu orbitals to the local environment [Fig. 10(a)]; the small differences in the Au region reflect, most likely, the greater sensitivity of the more diffuse Au orbitals to environmental charge fluctuations present in the SQS and missing in the SCPA. The near cancellation of charge-transfer effects on orbital energies (see Sec. III C 3) diminishes the overall effect of charge fluctuations on the DOS.

2. $Cu_{0.75}Pd_{0.25}$

The DOS of the *unrelaxed* $Cu_{0.75}Pd_{0.25}$ alloy is depicted in Figs. 9(a)–9(c), showing the results of the present SQS approach (solid lines) and previous KKR-CPA calculation of Ginatempo *et al.*[27] (dashed lines). In this unrelaxed geometry, the KKR-CPA calculation agrees remarkably with the present SQS results (requiring only an 8-atoms/cell calculation). The overall band widths and the major peak positions are in good agreement as in the case of $Cu_{0.75}Au_{0.25}$.

D. Effect of relaxation and comparison with experiment

1. $Cu_{0.75}Au_{0.25}$

Figures 12(a)–12(c) display the DOS of the relaxed disordered $Cu_{0.75}Au_{0.25}$ alloy, while Figs. 12(d)–12(f) shows the difference of DOS between the relaxed and unrelaxed $Cu_{0.75}Au_{0.25}$ alloy. The elongation of the "long bonds" (Cu–Au, Au–Au) due to structural relaxation [Fig. 6(b)] shifts the deep bonding states towards lower binding energy by $\sim$ 1 eV. The effect of relaxation on the Cu LDOS is again much smaller [Fig. 12(e)] than that of the Au LDOS.

Figure 13 compares our DOS with the experimental result of Krummacher *et al.*[47] using ultraviolet photoelectron spectroscopy (UPS). Figure 13(a) compares first the calculated DOS for the ordered $L1_2$ with experiment. In order to align the experimental and theoretical curves it was necessary to move rigidly the theoretical

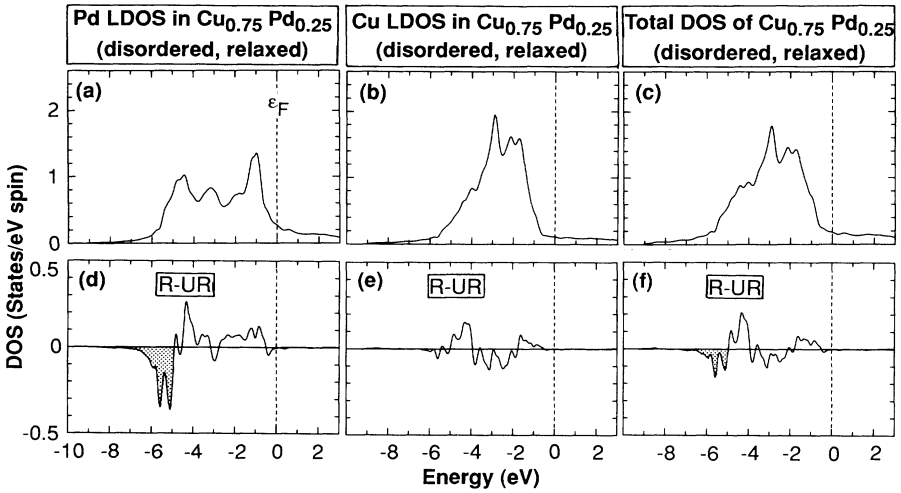

FIG. 14. (a)–(c) give the density of states of the relaxed disordered $Cu_{0.75}Pd_{0.25}$: (a) The Pd LDOS inside the muffin tin spheres. (b) The Cu LDOS inside the muffin-tin spheres. (c) Total DOS in the whole space. (d)–(f) shows the corresponding LDOS difference between the relaxed (R) and unrelaxed (UR) geometries.

curves for the Cu_3Au to higher binding energy by 0.6 eV.[47] We also apply this 0.6-eV shift to the calculated DOS of the disordered systems. Figure 13(a) shows that after applying this shift the DOS of the *ordered* compound agrees well with experiment (recall that symmetry does not permit the ordered $L1_2$ structure to relax). Figure 13(b) displays the calculated DOS for the *unrelaxed* $Cu_{0.75}Au_{0.25}$ alloy (thin line) and the experimental results (thick dotted line). Now there is a glaring discrepancy between experiment and theory: The unrelaxed calculation clearly overestimates the bandwidth by $\sim$ 1 eV [see the shaded region in Fig. 13(b)] as noted in previous CPA-KKR calculations.[47,60] This is mostly due to the overestimation of the Au binding energy as shown above. Figure 12 shows that relaxation narrows the $Cu_{0.75}Au_{0.25}$ DOS, especially in the Au bonding region. Inclusion of relaxation in the disordered alloy, neglected in SCPA calculations,[27,58–60] improves strikingly the agreement between the calculation and experiment[47] as shown in Fig. 13(c).

2. $Cu_{0.75}Pd_{0.25}$

Using the Cooper minimum in the photoelectron cross section, Wright *et al.*[72] were able to deduce the Cu and Pd LDOS's, finding that while the Cu LDOS agrees with the KKR-CPA calculation,[56] this calculation significantly overestimated the amplitude of the Pd LDOS in the high-binding-energy region ($\sim \varepsilon_F - 5.0$ eV). Wright *et al.*[72] had further suggested that the local bond-length expansion around the Pd site neglected in the SCPA calculations was probably the reason for this discrepancy. This overbinding of the Pd bonding state relative to experiment[72–76] in the Cu-rich Cu-Pd alloy appears to be a common problem among the calculations that assume a unique, unrelaxed single-bond length for Cu–Cu, Cu–Pd, and Pd–Pd.[27,54,56,77] Attempts to resolve this discrepancy have been made by applying phenomenological relaxation models, e.g., by Mašek and Kudrnovský,[55] Kudronovský and Drchal,[57] and by Stefanou *et al.*[78] Such relaxations are naturally described within the SQS method. The effect of relaxation on the DOS is illustrated in Fig. 14. It shows the DOS of the relaxed geometry [Figs. 14(a)–14(c)] and the difference between the relaxed and unrelaxed results [Figs. 14(d)–14(f)]. It clearly shows how relaxation removes intensity from the Pd LDOS region near $\varepsilon_F - 5$ eV, distributing it to lower binding energies [Fig. 14(d)]. This considerably improves the agreement with the photoemission data of Ref. 72. A similar effect is seen at the composition $Cu_{0.5}Pd_{0.5}$ (Fig. 15). Note that relaxation has a much smaller effect on the Cu LDOS [Fig. 14(e)], for which good agreement with experiment exists already for the unrelaxed geometry.

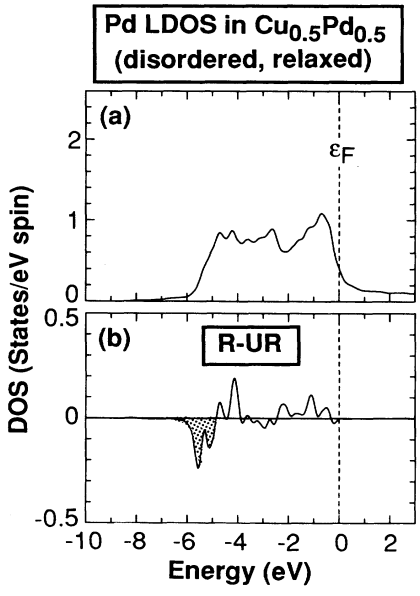

FIG. 15. (a) gives the PD LDOS inside the muffin-tin sphere of the relaxed disordered $Cu_{0.5}Pd_{0.5}$. (b) shows the LDOS difference between the relaxed (R) and the unrelaxed (UR) geometries.

TABLE VI. Comparison of the density of states at Fermi energies for ordered $L1_2$ and random Cu_3X alloys, in units of states/eV spin.

	$L1_2$		Random, unrelaxed		Random, relaxed	
	No S-O	With S-O	No S-O	With S-O	No S-O	With S-O
			Cu_3Au			
Present	0.123	0.124	0.149	0.155	0.150	0.152
LMTO[a]	0.128	0.129				
LMTO[b]	0.142					
			Cu_3Pd			
Present	0.214		0.183		0.181	
KKR[c]			0.150			

[a]Reference 30 using a non-self-consistent linearized muffin-tin orbital (LMTO) method within the atomic-sphere approximation (ASA) and at the lattice constant of $a = 3.748$ Å.
[b]Reference 32 using a self-consistent LMTO method within ASA and the von Barth–Hedin exchange correlation potential (Ref. 22) at the lattice constant of $a = 3.7426$ Å.
[c]Reference 56 using a self-consistent KKR-CPA method and the von Barth–Hedin exchange-correlation potential at the lattice constant of $a = 3.681$ Å.

E. Explanation of relaxation effects in $Cu_{0.75}Au_{25}$ and $Cu_{0.75}Pd_{25}$

The reason for these selective, relaxation-induced shifts can be understood from Figs. 2 and Fig. 6, as follows.

(i) Figure 6 shows that relative to the unrelaxed geometry, relaxation *increases* the length of the Cu–Pd and Pd–Pd bonds in Cu-Pd (and the Cu–Au and Au–Au distances in Cu-Au), while *reducing* the length of the Cu–Cu bonds.

(ii) The deep Pd state in Cu-Pd near $\varepsilon_F - 5$ eV has a *bonding* character. The same is true for the deep Au states in Cu-Au near $\varepsilon_F - 7$ eV [Fig. 5(a)].

(iii) Bonding states shift to *lower* binding energies as the underlying bond becomes *longer*. This can be seen in Fig. 2(b): When the lattice constant of pure Pd is increased from a smaller value (appropriate to that of Cu_3Pd, dashed line) to a longer value (the calculated Pd lattice constant, solid line), the bonding states near $\varepsilon_F - 5$ eV shift to lower binding energies by ~ 1.5 eV. Conversely, Fig. 2(a) shows that when the lattice constant of pure Cu is *reduced* (compare dashed line with solid line), the binding energy *increases*. The effect is much smaller for the Cu states on account of its more compact $3d$ orbitals. The same effects are evident in Fig. 2(c) for the Cu-Au case.

This analysis shows that the relaxation-induced increase in the Cu–Pd and Pd–Pd bond lengths (or the Cu–Au and Au–Au bonds, as seen in Fig. 6) is the primary reason for the significant shift of the Pd (or Au) bonding state to lower binding energies [Fig. 14(d) and Fig. 15(b)]. The extent to which the dilation of bond lengths (Cu–Pd and Pd–Pd) shift the Pd bonding state to lower binding energies is smaller in the $Cu_{0.5}Pd_{0.5}$ alloy. This shift is smaller and weaker in intensity in the case of $Cu_{0.5}Pd_{0.5}$: As seen in Fig. 15, relaxation shifts the Pd bonding states to lower binding energies only by $\sim$ 0.4 eV and the LDOS difference [Fig. 15(b)] is considerably smaller than in the case of $Cu_{0.75}Pd_{0.25}$ [Fig. 14(d)]. This can be understood from Fig. 6(a), where we plot the average bond lengths in $Cu_{1-x}Pd_x$. The elongation of the Cu–Pd and Pd–Pd bond length with respect to the virtual-crystal average [Eq. (13)] are larger in $Cu_{0.75}Pd_{0.25}$ than in $Cu_{0.5}Pd_{0.5}$ [i.e., the changes are +1.4% and +0.5% (Cu–Pd bond) and +2.1% and +1.8% (Pd–Pd bond) for $Cu_{0.75}Pd_{0.25}$ and $Cu_{0.5}Pd_{0.5}$, respectively]. Hence, the bonding states in $Cu_{0.5}Pd_{0.5}$ are shifted less than in $Cu_{0.75}Pd_{0.25}$.

F. DOS at the Fermi energy

The density of states at the Fermi energy (ε_F) is related to electronic specific heat. Table VI lists the density of states at Fermi energy $D(\varepsilon_F)$ for both ordered and disordered Cu-Au and Cu-Pd systems. We notice that ordering reduces the value of the $D(\varepsilon_F)$ of Cu_3Au by $\sim$ 20%. This is consistent with experimental specific heat measurements.[32] Interestingly, ordering has an opposite effect on $D(\varepsilon_F)$ for Cu_3Pd system: it increases the $D(\varepsilon_F)$ by $\sim$ 16%.

VIII. SUMMARY

The single, unique chemical environment of the Cu and X atoms in the ordered $L1_2$ structure of Cu_3X is replaced in the disordered $Cu_{0.75}X_{0.25}$ alloy by a broad distribution of local coordination shells. Chemically identical atoms are now experiencing a distribution of different types of neighbors. This drives fluctuations in the local charge transfer, local site symmetries, and bond lengths. While relatively compact d orbitals (e.g., Cu $3d$) have only a limited ability to sense the altered local environments, the more diffuse Pd $4d$ and Au $5d$ orbitals, sensitively respond to these fluctuations. The homogeneous site-coherent-potential approximation (SCPA) limits these fluctuations to a single site; hence, only the *average* changes are recorded. In the special quasirandom structure (SQS) method, we do not require that each atom "see" an identical, average medium. Instead, we create a distribution of distinct local environments that reproduce the correct short-range correlation functions

of an infinite random network. Application to Cu-Pd and Cu-Au shows that concomitantly with the creation of a distribution of inequivalent sites in the random alloy, there is a distribution of local charges and bond lengths. In the *unrelaxed* SQS approximation, the various atoms are not permitted to respond to this symmetry lowering. In this high-enthalpy "excited-state" configuration the SQS and the CPA produce rather similar density of states, especially in the spectral regions where localized, environmentally insensitive orbitals exist. As this geometrical constraint is removed, the atoms in the alloy are found to relax massively in a nonhydrostatic fashion, lowering the energy by $\sim 30\%$. This relaxation lifts the artificial restriction $R_{\mathrm{Cu-Cu}} = R_{\mathrm{Cu}-X} = R_{X-X}$ underlying the CPA: Three *distributions* of inequivalent Cu–Cu, Cu–X, and X–X bond lengths are created. Concomitantly, the Cu-X and X-X bonding states (whose bond lengths are now elongated) shift to lower binding energies by as much as ~ 1 eV, removing much of the previously noted discrepancy with the measured photoemission spectra.

ACKNOWLEDGMENTS

We wish to thank Dr. G. S. Sohal for providing some of the references on Cu_3Au system and Dr. Ginatempo for providing us their DOS of $Cu_{0.75}Pd_{0.25}$ (Fig. 9) for comparison. This work was supported by the Office of Energy Research (OER) [Division of Materials Science of the Office of Basic Science (BES)], U. S. Department of Energy, under Contract No. DE-AC02-77-CH00178.

[1] P. M. Hansen, *Constitution of Binary Alloys* (McGraw-Hill, New York, 1958).
[2] R. Hultgren, P. D. Desai, D. T. Hawkins, M. Gleiser, and K. K. Kelley, *Selected Values of the Thermodynamics Properties of Binary Alloys* (American Society for Metals, Metals Park, OH, 1973).
[3] *Binary Alloy Phase Diagrams*, edited by J. L. Murray, L. H. Bennett, and H. Barker (American Society for Metals, Metals Park, OH, 1986).
[4] *Phase Diagrams of Binary Gold Alloys*, edited by H. Okamoto and T. B. Massalski (ASM International, Materials Park, Ohio, 1987).
[5] Z. W. Lu, S.-H. Wei, A. Zunger, S. Frota-Pessoa, and L. G. Ferreira, Phys. Rev. B **44**, 512 (1991).
[6] Z. W. Lu, S.-H. Wei, A. Zunger, L. G. Ferreira, Solid State Commun. **78**, 583 (1991).
[7] B. Velický, S. Kirkpatrick, and H. Ehrenreich, Phys. Rev. **175**, 747 (1968).
[8] P. Soven, Phys. Rev. **178**, 1136 (1969).
[9] A. Zunger, S.-H. Wei, L. G. Ferreira, and J. E. Bernard, Phys. Rev. Lett. **65**, 353 (1990).
[10] S.-H. Wei, L. G. Ferreira, J. E. Bernard, and A. Zunger, Phys. Rev. B **42**, 9622 (1990); S. H. Wei and A. Zunger, *ibid.* **43**, 1662 (1991); R. Magri, S. Froyen, and A. Zunger, *ibid.* **44**, 7949 (1991).
[11] K. C. Hass, L. C. Davis, and A. Zunger, Phys. Rev. B **42**, 3757 (1990).
[12] S.-H. Wei and H. Krakauer, Phys. Rev. Lett. **55**, 1200 (1985), and references therein.
[13] Z. W. Lu, S.-H. Wei, and A. Zunger, Phys. Rev. B **44**, 3387 (1991).
[14] P. Hohenberg and W. Kohn, Phys. Rev. **136**, B864 (1964).
[15] W. Kohn and L. J. Sham, Phys. Rev. **140**, A1133 (1965).
[16] E. Wigner, Phys. Rev. **46**, 1002 (1934).
[17] H. J. Monkhorst and J. D. Pack, Phys. Rev. B **13**, 5188 (1976).
[18] G. Lehman and M. Taut, Phys. Status Solidi **54**, 469 (1971).
[19] R. W. G. Wyckoff, *Crystal Structure* (Interscience, New York, 1963), Vol. 1.
[20] P. Villars and L. Calvert, *Pearson's Handbook of Crystallographic Data for Intermetallic Phases* (American Society for Metals, Metals Park, Ohio, 1985).
[21] S. Takizawa and K. Terakura, Phys. Rev. B **39**, 5792 (1989).
[22] U. von Barth and L. Hedin, J. Phys. C **5**, 1629 (1972).
[23] J. W. Davenport, R. E. Watson, and M. Weinert, Phys. Rev. B **37**, 9985 (1988).
[24] L. Hedin and B. I. Lundqvist, J. Phys. C **4**, 2063 (1971).
[25] For Ni-Pt in the $L1_0$ structure, we find $\Delta H_{\mathrm{SR}} = -93.6$ meV/atom, while $\Delta H_{\mathrm{NR}} = +143.9$ meV/atom; see Z. W. Lu, S.-H. Wei, and A. Zunger, Phys. Rev. Lett. **68**, 1961 (1992).
[26] P. J. Durham, C. F. Hague, J.-M. Mariot, and W. M. Temmerman, J. Phys. (Paris) Colloq. **48**, C9-1059 (1987).
[27] B. Ginatempo, G. Y. Guo, W. M. Temmerman, J. B. Staunton, and P. J. Durham, Phys. Rev. **42**, 2761 (1990).
[28] D. A. Papaconstantopoulos, A. Gonis, and P. M. Laufer, Phys. Rev. B **40**, 12196 (1989).
[29] D. Gray and E. Brown, Phys. Rev. **160**, 567 (1967).
[30] H. L. Skriver and H. P. Lengkeek, Phys. Rev. B **19**, 900 (1979).
[31] P. Weinberger, A. M. Boring, R. C. Albers, and W. M. Temmerman, Phys. Rev. B **38**, 5357 (1988).
[32] K. Kokko, E. Ojala, K. Mansikka, J. Phys. Condens. Matter **2**, 4587 (1990).
[33] J. Kudrnovský, S. K. Bose, and O. K. Andersen, Phys. Rev. B **43**, 4613 (1991).
[34] R. G. Jordan, G. S. Sohal, B. L. Gyorffy, P. J. Durham, W. M. Temmerman, and P. Weinberger, J. Phys. F **15**, L135 (1985).
[35] Z. Q. Wang, S. C. Wu, J. Quinn, C. K. C. Lok, Y. S. Li, and F. Jona, Phys. Rev. B **38**, 7442 (1988).
[36] G. K. Wertheim, L. F. Mattheiss, and D. N. E. Buchanan, Phys. Rev. B **38**, 5988 (1988).
[37] G. S. Sohal, C. Carbone, E. Kisker, S. Krummacher, A. Fattah, W. Uelhoff, R. C. Albers, and P. Weinberger, Z. Phys. B **78**, 295 (1990).
[38] J. A. Catterall and J. Trotter, Proc. Phys. Soc. **79**, 691 (1962).
[39] P.-O. Nilsson and C. Norris, Phys. Lett. **29A**, 22 (1969).
[40] W. Scott and L. Muldawer, Phys. Rev. B **9**, 1115 (1974).
[41] P. P. Deimel, R. J. Higgins, and R. K. Goodall, Phys. Rev. B **24**, 6197 (1981).
[42] P. P. Deimel and R. J. Higgins, Phys. Rev. B **25**, 7117 (1982).
[43] T. Cleason and J. B. Boyce, Phys. Rev. B **29**, 1551 (1984).
[44] W. Eberhardt, S. C. Wu, R. Garrett, D. Sondericker, and

F. Jona, Phys. Rev. B **31**, 8285 (1985).
[45] S. B. DiCenzo, P. H. Citrin, E. H. Hartford, Jr., and G. K. Wertheim, Phys. Rev. B **34**, 1343 (1986).
[46] G. K. Wertheim, Phys. Rev. B **36**, 4432 (1987).
[47] S. Krummacher, N. Sen, W. Gudat, R. Johnson, F. Grey, and J. Ghijsen, Z. Phys. B **75**, 235 (1989).
[48] T. K. Sham, K. H. Tan, and Y. M. Yiu, Physica B **158**, 28 (1989).
[49] A. Stuck, J. Osterwalder, T. Greber, S. Hüfner, and L. Schlapbach, Phys. Rev. Lett. **65**, 3029 (1990).
[50] M. Kuhn, T. K. Sham, J. M. Chen, and K. H. Tan, Solid State Commun. **75**, 861 (1990).
[51] T. K. Sham, Y. M. Yiu, M. Kuhn, K. H. Tan, Phys. Rev. B **41**, 11 881 (1990).
[52] V. L. Moruzzi, A. R. Williams, and J. F. Janak, Phys. Rev. B **10**, 4856 (1974).
[53] A. Bansil, Phys. Rev. B **20**, 4025 (1979); **20**, 4035 (1979).
[54] J. Kudrnoský and J. Mašek, Phys. Rev. B **31**, 6424 (1985).
[55] J. Mašek and J. Kudrnovský, Solid State Commun. **58**, 67 (1986); J. Phys. Chem. Solids **49**, 349 (1988).
[56] H. Winter, P. J. Furham, W. M. Temmerman, and G. M. Stocks, Phys. Rev. B **33**, 2370 (1986).
[57] J. Kudrnovský and V. Drchal, Solid State Commun. **70**, 577 (1989); Phys. Rev. B **41**, 7515 (1990).
[58] E. Arola, R. S. Rao, and A. Salokatve, Phys. Rev. B **41** 7361 (1990).
[59] I. A. Abrikosov, Y. H. Vekilov, and A. V. Ruban, Phys. Lett. A **154**, 407 (1991).
[60] B. Ginatempo and J. B. Staunton, J. Phys. F **18**, 1827 (1988).
[61] G. Renaud, N. Motta, F. Lancon, and M. Belakhovsky, Phys. Rev. B **38**, 5944 (1988).
[62] P. Weightman, H. Wright, S. D. Waddington, D. van der Marel, G. A. Sawatzky, G. P. Diakun, and D. Norman, Phys. Rev. **36**, 9098 (1987).
[63] Z. W. Lu, S.-H. Wei, and A. Zunger, Phys. Rev. B **44**, 10 470 (1991).
[64] *International Tables for Crystallography*, edited by T. Hahn (Deidel, Dordrecht, 1983), p. 150.
[65] D. M. Wood and A. Zunger, Phys. Rev. B **40**, 4062 (1989).
[66] R. Yu, D. Singh, and H. Krakauer, Phys. Rev. B **43**, 6411 (1991).
[67] In Refs. 5 and 6, we have calculated the mixing enthalpies of ten ordered structures and extracted the renormalized Ising-interaction energies, and we were able to predict the mixing enthalpies of the random alloy. For Cu-Pd at $x = \frac{1}{2}$, we found $\Delta H^{\rm UR}_{\rm mix}(\frac{1}{2}) \sim -48$ meV/atom and $\Delta H^{\rm R}_{\rm mix}(\frac{1}{2}) \sim -77$ meV/atom. For the unrelaxed system, we see quite good agreement between the cluster expansion (above) and present direct SQS calculations (see text). The agreement is worse for the relaxed results owing to the slower convergence in the cluster expansion.
[68] L. Pauling, *The Nature of the Chemical Bond*, 3rd ed. (Cornell University Press, Ithaca, 1960), p. 93.
[69] R. E. Watson, M. Weinert, and G. M. Fernando, Phys. Rev. B **43**, 1446 (1991).
[70] J. Hedman, M. Klasson, R. Nilsson, and C. Nordling, Phys, Scr. **4**, 195 (1971).
[71] R. Magri, S.-H. Wei, and A. Zunger, Phys. Rev. B **42**, 11 388 (1990).
[72] H. Wright, P. Weightman, P. T. Andrews, W. Folkerts, C. F. J. Flipse, G. A. Sawatzky, D. Norman, and H. Padmore, Phys. Rev. B **35**, 519 (1987).
[73] S. Hüfner, G. K. Wertheim, and J. H. Wernick, Solid State Commun. **17**, 1585 (1975).
[74] N. Mårtensson, R. Nyholm, H. Calén, J. Hedman, and B. Johansson, Phys. Rev. B **24**, 1725 (1981).
[75] D. van der Marel, J. A. Jullianus, and G. A. Sawatzky, Phys. Rev. B **32**, 6331 (1985).
[76] M. Davies and P. Weightman, J. Phys. C **17**, L1015 (1984).
[77] P. J. Braspenning, R. Zeller, P. H. Dederichs, and A. Lodder, J. Phys. F **12**, 105 (1982); P. J. Braspenning, R. Zeller, A. Lodder, and P. H. Dederichs, Phys. Rev. B **29**, 703 (1984).
[78] N. Stefanou, R. Zeller, and P. H. Dederichs, Solid State Commun. **62**, 735 (1987); N. Stefanou, P. J. Braspenning, R. Zeller, and P. H. Dederichs, Phys. Rev. B **36**, 6372 (1987).

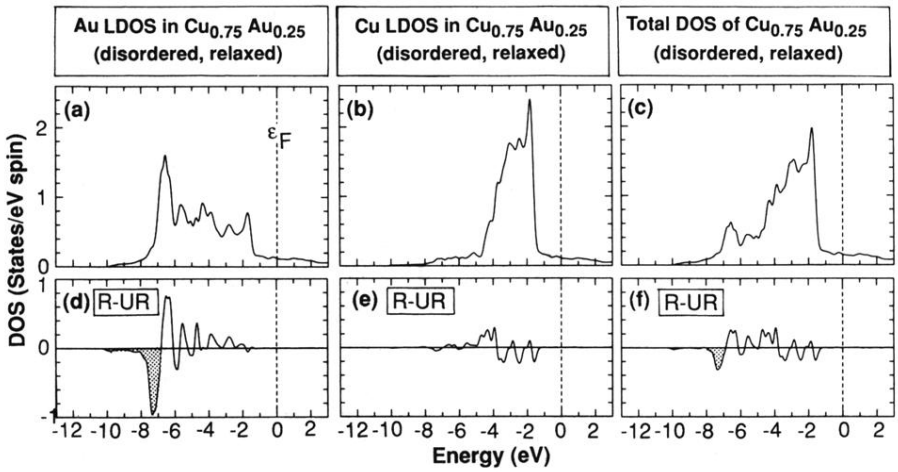

FIG. 12. (a)–(c) give the density of states of the relaxed disordered $Cu_{0.75}Au_{0.25}$. (a) LDOS inside the Au muffin-tin spheres. (b) LDOS inside the Cu muffin-tin spheres. (c) total DOS in the whole space. (d)–(f) shows the corresponding LDOS difference between the relaxed (R) and unrelaxed (UR) geometries. The fully relativistic calculation was carried out at $\overline{a} = 3.709$ Å.

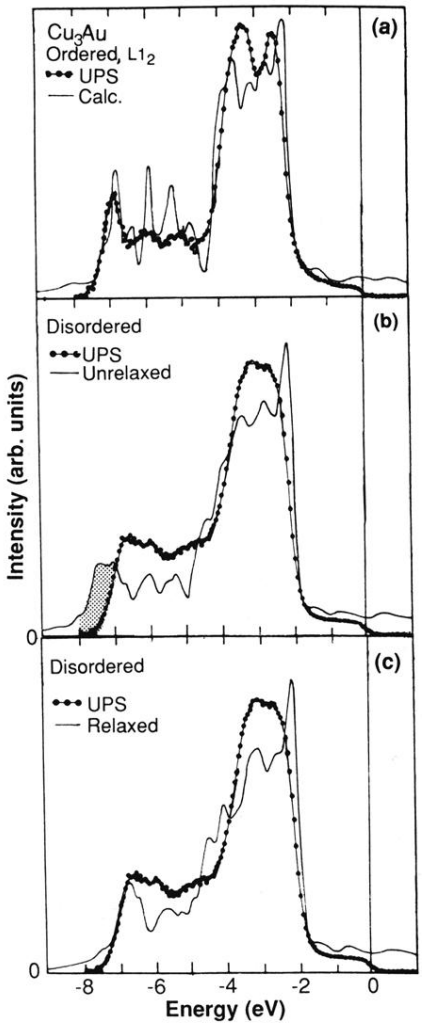

FIG. 13. Comparison between our fully relativistic DOS and the measured valence band photoemission (UPS) (Ref. 47) for Cu_3Au. The thin lines represent the calculated results, while the connected dotted lines represent the experimental results. (a) The ordered $L1_2$ Cu_3Au calculated at $a = 3.743$ Å. (b) The unrelaxed $Cu_{0.75}Au_{0.25}$ DOS calculated at $a = 3.755$ Å. (c) The relaxed $Cu_{0.75}Au_{0.25}$ DOS calculated at $a = 3.755$ Å. The shaded area in (b) highlights the $\sim$ 1-eV discrepancy with experiment, which is rectified by including relaxation (c).

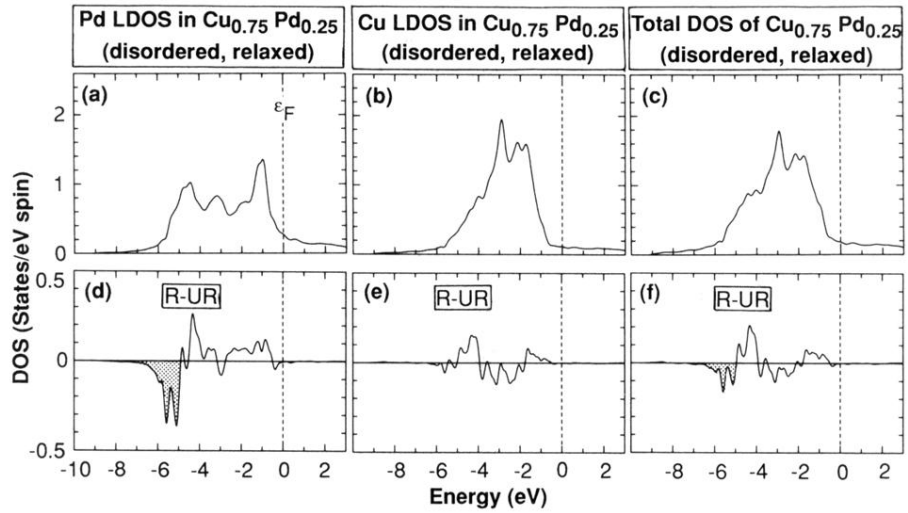

FIG. 14. (a)–(c) give the density of states of the relaxed disordered $Cu_{0.75}Pd_{0.25}$: (a) The Pd LDOS inside the muffin tin spheres. (b) The Cu LDOS inside the muffin-tin spheres. (c) Total DOS in the whole space. (d)–(f) shows the corresponding LDOS difference between the relaxed (R) and unrelaxed (UR) geometries.

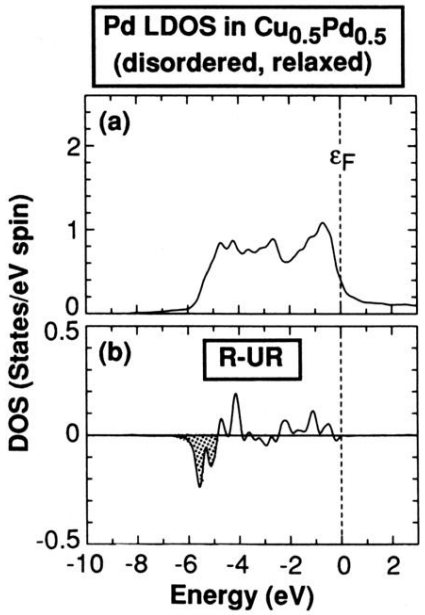

FIG. 15. (a) gives the PD LDOS inside the muffin-tin sphere of the relaxed disordered $Cu_{0.5}Pd_{0.5}$. (b) shows the LDOS difference between the relaxed (R) and the unrelaxed (UR) geometries.

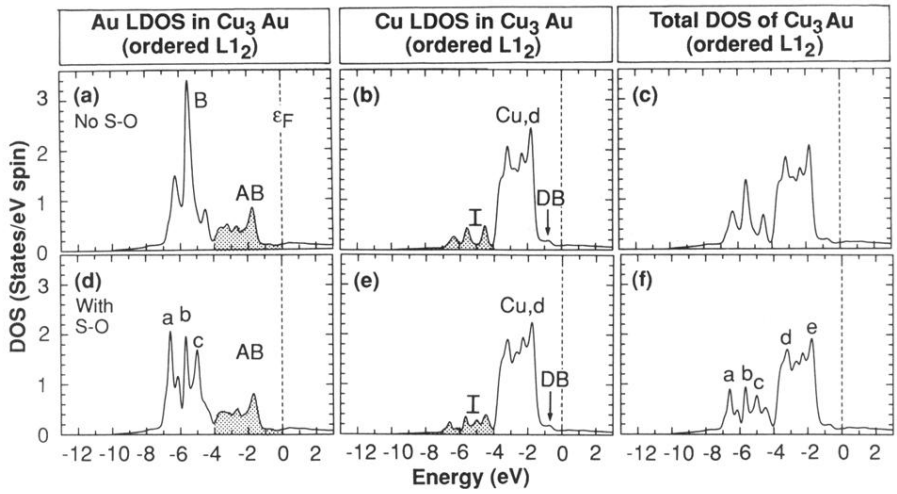

FIG. 3. DOS of ordered $L1_2$ Cu_3Au (a) inside the Au muffin-tin spheres (b) inside the Cu muffin-tin spheres. (c) Total DOS in the whole space. The calculation was carried out at $\overline{a} = 3.709$ Å. Results for (a)–(c) are scalar relativistic (without spin-orbit effects). Panels (d)–(f) show the corresponding results including spin-orbit effects. The capital letters denote type of states: B=bonding, AB=anti-bonding, I=induced, DB=dangling bond (see text). The lower-case letters a, b, c, d, and e denote peak positions whose energies are given in Table III.